A FREEZE PRECONCENTRATION METHOD AND A LONG ABSORPTION CELL FOR ATOMIC ABSORPTION SPECTROSCOPY

BY

WENG-JANG WANG

A DISSERTATION PRESENTED TO THE GRADUATE SCHOOL
OF THE UNIVERSITY OF FLORIDA IN
PARTIAL FULFILLMENT OF THE REQUIREMENTS
FOR THE DEGREE OF DOCTOR OF PHILOSOPHY

UNIVERSITY OF FLORIDA

1986

To my parents, for their love.

ACKNOWLEDGMENTS

I would like to express my deep gratitude and appreciation to my research director, Professor James D. Winefordner, for his patience, encouragement and guidance during the course of this work. I would also like to acknowledge the members of my supervisory committee for their valuable time.

I wish to give special thanks to Dr. Shigeki Hanamura for his help, friendship and valuable discussions on the research.

The friendship and cooperation provided by my colleagues in the spectroscopy group are greatly appreciated.

I would like to thank my husband, Jen-Chi, and my daughter, Ida, for their patience and understanding.

TABLE OF CONTENTS

Page

ACKNOWLEDGMENTS....................iii

LIST OF TABLES....................v

LIST OF FIGURES....................vii

ABSTRACT....................xi

CHAPTERS

I GENERAL INTRODUCTION....................1

II FREEZE PRECONCENTRATION METHOD....................3

- Background Introduction....................3
- Fundamental Considerations....................15
- Experimental Section....................26
- Results and Discussion....................42

III DEVELOPMENT OF LONG ABSORPTION CELL FOR ATOMIC ABSORPTION SPECTROSCOPY....................74

- Background Introduction....................74
- Theoretical Considerations....................93
- Experimental Section....................101
- Results and Discussion....................112

IV SUMMARY AND CONCLUSIONS....................161

- Freeze Preconcentration Method....................161
- Long Absorption Cell AAS....................162

REFERENCES....................164

BIOGRAPHICAL SKETCH....................169

LIST OF TABLES

Table Page

1 Comparison of the Effects of Freeze Preconcentration and Vacuum Preconcentration on the Refractive Index, Sugar Content, Acid Content, Ascorbic Acid Content, and Aroma Compounds Content....6

2 Average Losses of Volatiles from Fruit Juice Concentrates Prepared by Five Different Methods...7

3 Concentration Costs per 1000 kg of Water Removed for Various Processes Operated for 60 and 220 Days....9

4 Comparison of Freeze Preconcentration and Freeze Drying Processes....11

5 Application of Freeze Preconcentration Process in Analytical Chemistry....14

6 Physical Meaning of Equation Parameters....24

7 Instrument Settings for Graphite Furnace Atomic Absorption Spectrometer....31

8 Recovery of Lead Arsenate from Deionized Water with 4-Fold Freeze Preconcentration....43

9 Recovery of Lead Arsenate from Deionized Water and Tap Water with 20-Fold Freeze Preconcentration....44

10 Comparison of Emission Intensities of Four Bromine Emission Lines for $C_2H_4Br_4$ in the Single Electrode Microwave Plasma....59

11 Comparison of Dimensions of Electrothermal Tube Furnaces....77

12 Peak Height and Peak Area Absorbance for 0.5 ng of Lead in Aqueous Solution and in the Presence of 1 μg of Sodium Nitrate, Respectively....83

13 Comparison of Detection Limits for Electrothermal Vaporization and Pneumatic Nebulization from Previous Studies...............89

14 Instrument Settings of Long Absorption Cell Hitachi Atomic Absorption Spectrometer System...105

15 Instrument Setting for Hitachi Flame Atomic Absorption Spectrometry.........................109

16 Comparison of Detection Limits (ng/mL) for Analytical Atomic Spectrometric Method Utilizing Hydride Generation....................119

17 Arsenic and Antimony Content of NBS Standard Reference Materials Measured by Collection Hydride Generation and Long Absorption Cell Atomic Absorption Spectrometry..................120

18 Permissible Concentration Ratio of Interferent, I, to Analyte, A (I/A).............134

LIST OF FIGURES

Figure Page

1 Phase diagram for a simple binary system.........18

2 Real ice/container system during the solidification in cooled container and correspondent virtual system..................................22

3 Cylindrical-ice formation $r^* \leq 1$ and thermal-circuit representation..........................23

4 Cross-sectional view of freeze preconcentration system..28

5 Block diagram of Evolved Gas Analysis/Single Electrode Microwave Plasma Emission Spectrometer (EGA/SEMPES).....................................33

6 Schematic diagram of the single electrode microwave plasma torch...........................35

7 Schematic diagram of induction furnace vaporization system...............................37

8 Schematic diagram of electric resistance furnace vaporization system......................39

9 Evolution temperature profiles for Pb and O from $PbHAsO_4$....................................50

10 Evolution temperature profiles for Pb and H from $PbHAsO_4$....................................52

11 Evolution temperature profiles for Pb and As from $PbHAsO_4$....................................54

12 Emission spectra (400-900 nm) of Br in single electrode microwave plasma.......................58

13 Microwave emission analytical calibration curve of $C_2H_4Br_4$ introduced into single electrode microwave plasma.......................61

14 Comparison of Br emission signals for $C_2H_4Br_2$ in several different solutions....................63

15 Comparison of Br emission signals for $C_2H_4Br_2$ for several different conditons..................66

16 Comparison of loss of $C_2H_4Br_2$ at 15 min stirring intervals...............................68

17 Decay of $C_2H_4Br_2$ by stirring of solution.........70

18 Single electrode microwave emission of Br, C and H in $C_2H_4Br_2$ by thermal gas evolution..73

19 Electrothermal atomizer chambers used in atomic absorption spectrometry....................76

20 Variation with time of the varian furnace surface temperature along with the length of the graphite tube at a furnace heating rate of 1.10 kms^{-1}....................................80

21 Effect of the heating rate on the maximum atom population, N_{max}, with activation energy as parameter..............................85

22 Effect of the tube length on the maximum atom population, N_{max}, with activation energy as a parameter...................................87

23 Variation in the number of atoms in an analysis volume for different ratio t_1/t_2........97

24 Furnace atomizer absorbance-time profile........100

25 Cross-sectional view of long absorption cell....104

26 Block diagram of arsine and stibine generation system...............................107

27 Comparison of sample introduction methods for 10 ng As..................................114

28 Comparison of sample introduction methods for 10 ng Sb..................................116

29 Absorption vs time plots obtained by the direct transfer mode for 500 ng of each element except bismuth (100 ng).................117

30 Effect of helium flow rate on peak height absorption signal for collection mode-hydride generation-long absorption cell atomic absorption spectrometry..........................123

31 Effect of argon flow rate on peak height absorption signal for collection mode-hydride generation-long absorption cell atomic absorption spectrometry..........................125

32 Effect of trapping time on peak height absorption signal for collection mode-hydride generation-long absorption cell atomic absorption spectrometry..........................127

33 Effect of trapping time and U-tube traps on Sb (217.5 nm) for collection mode-hydride generation-long absorption cell atomic absorption spectrometry..........................130

34 Emission signals of H_2 and SbH_3 as a formation of $NaBH_4$/HCl reaction time......................132

35 Effect of interferent on the determination of analyte (10 ng)..............................136

36 Effect of furnace temperature on the absorption signal for As 10 ng (Δ) and Sb 10 ng (○) with long absorption cell atomic absorption spectrometry....................................139

37 Effect of inner tube in long absorption cell on the absorption signal of Sb (10 ng)..........141

38 Effect of inner tube in long absorption cell on the absorption signal of As (10 ng)..........143

39 Absorption signal for As (10 ng) in long absorption cell without the Zeeman effect (a) and with the Zeeman effect (b)..................146

40 Absorption signal for Sb (10 ng) in long absorption cell without the Zeeman effect (a) and with the Zeeman effect (b)..................148

41 Zeeman splitting pattern for As 193.7 nm and Sb 217.5 nm..................................150

42 Analytical calibration curves for As (193.7 nm)......................................154

43 Analytical calibration curves for Sb (217.5 nm)....................................156

44 Antimony absorption signal (217.5 nm) for 100 ng Sb (a) and 1000 ng Sb (b) in long absorption cell...............................159

Abstract of Dissertation Presented to the Graduate School
of the University of Florida in Partial Fulfillment of the
Requirements for the Degree of Doctor of Philosophy

A FREEZE PRECONCENTRATION METHOD AND A LONG ABSORPTION CELL FOR ATOMIC ABSORPTION SPECTROSCOPY

BY

WENG-JANG WANG

December, 1986

Chairman: Dr. James D. Winefordner
Major Department: Chemistry

This dissertation includes two parts: a freeze preconcentration method and a long absorption cell for atomic absorption spectroscopy.

The aim of the first part of this research is to evaluate the freeze preconcentration process as a sample pretreatment method. A simple freeze preconcentration apparatus is constructed to determine the possibility for applying this technique for analytical purposes. Optimum conditions and their correlation with the rate of ice formation are then described. The recoveries of two analytes, lead arsenate ($PbHAsO_4$) and ethylene dibromide ($C_2H_4Br_2$), in deionized water and tap water, are also investigated. The concentrations of Pb and As are determined by graphite furnace atomic absorption spectroscopy, while $C_2H_4Br_2$ is detected by single electrode microwave plasma emission spectroscopy. The limitations of the freeze preconcentration process for volatile species, which include large losses, are discussed.

The purpose of the second part of this investigation is to develop a long absorption cell for atomic absorption spectrometry and to appraise its usefulness. This long absorption cell includes a gas sample inlet tube and a 14 cm graphite device which fit into a commercial atomic absorption spectrometer.

Arsine or stibine is generated in a round bottom flask using $NaBH_4$-acid solution. Helium gas carries the hydrides from a liquid nitrogen trap into the interior of an aluminum tube, which is located within the graphite tube furnace. Optimum hydride reaction, trapping and carrier gas flow rate conditions for arsine and stibine are studied. Furthermore, interelement interferences, furnace temperature, presence of an inner tube, and Zeeman background correction effects are investigated. Comparisons between conventional flame atomic absorption spectrometry, conventional graphite furnace atomic absorption spectrometry, and long absorption cell atomic absorption spectrometry are given. Detection limits and analytical useful ranges for As and Sb are 0.2 ng/mL and 0.1 ng/mL and 3 to 4 orders of magnitude for both, respectively. Arsenic and antimony are determined in various NBS reference materials, and the precision and accuracy of the measurement are also discussed.

CHAPTER I
GENERAL INTRODUCTION

The general case in analytical chemistry is that samples with or without pretreatment are analyzed by a suitable instrument and procedure. Thus, there are two ways which can be tried to improve the measurement sensitivity of the system: first, sample pretreatment, in which sample is preconcentrated to lower the concentration limit of detection; and second, improvement of the instrument by using more suitable materials or more sensitive detection devices.

This dissertation includes two parts. The first part of the research is to evaluate the freeze preconcentration process, which is a sample pretreatment method. The freeze preconcentration technique developed here involves concentration of a liquid sample by partial freezing and separation of the resulting pure ice crystals. This technique is finding increasing use in many application areas including the food, pharmaceutical, and other industries, but it has not been routinely used by analysts, and references to its use in the laboratory are rare. The introduction of a freeze concentration technique and the theoretical considerations are given in Chapter II along with the discussions of experiments and results. In the second part, a sensitive method for the determination of arsenic and antimony involving hydride generation and atomic absorption spectroscopy with an improved long tube graphite furnace is developed. The graphite furnace atomic absorption spectrometry and hydride generation system, the fundamental considerations, and the discussion of experiments and results will be given in Chapter III. The conclusions for these two methods will be given in Chapter IV.

CHAPTER II
FREEZE PRECONCENTRATION METHOD

Background Introduction

History of Freeze Preconcentration Technique

The process of freeze concentration is almost a century old. The three oldest studies were reported in 1868, 1871, and 1894, in which the preconcentration of alcohol, saline water, and milk, respectively, were described (1). Since those studies, hundreds of patents on freeze concentration concepts have been obtained in the world's industrialized countries. Preconcentration makes possible

a. improvement in product stability and shelf life;
b. reduced requirements for storage;
c. reduced refrigeration;
d. reduced transport costs;
e. more profitable export marketing; and
f. production at full capacity for year-round availability.

A typical freeze preconcentration system consists of three components: freezer, separation device, and refrigeration unit. The principle of freeze concentration is to enable the separation of solid crystals based upon liquid-solid phase equilibrium. The fundamental considerations will be discussed in more detail in the next section.

Freeze preconcentration is free from the drawbacks associated with evaporation. It is capable of concentrating liquids without deteriorating flavor, aroma, color, and nutritive value, and does not alter the chemical and physical properties of the substances (2).

Freeze preconcentration was not widely used in industrial applications until the early 1960s. The two main factors which contributed to nonacceptance of this technique in the past were economics and that no practical, reliable, commercial-scale freeze concentration plant was available in the early 1960s.

Freeze preconcentration is and will be an attractive process, at least in coming years, in the production of freeze-dried fruit, coffee, instant tea, and for the desalination of seawater. It can prove of greatest value for biological materials, pharmaceuticals, biochemical products, and food stuffs. It is especially suitable for concentrating chemicals which are heat-labile, such as enzyme preparations. Nevertheless, in the food industry, especially in the preconcentration of food liquid, freeze concentration still appears to be an uneconomic process; the cost of the technique must be further reduced through the development of newer and cheaper designs (3).

The application of freeze preconcentration in analytical chemistry will be discussed in a latter section.

Advantages and Disadvantages

Freeze preconcentration has several advantages over other preconcentration processes such as evaporation and reverse osmosis. Some of the advantages claimed (2) are given below:

a. Liquids may be preconcentrated without loss in taste, aroma, color, and nutritive value. Table 1 presents the study by Almasi and Perjes (4), who compared the effects of the freeze preconcentration and vacuum evaporation processes based upon refractive index change, total sugar content, acid content, ascorbic acid content, and content of aromatic compounds. The results show that both the ascorbic and aromatic compounds were more effectively preserved during freeze concentration than during vacuum evaporation preconcentration. Table 2 shows the results by Bolin (5), who studied the losses of volatiles from apple, cherry, and peach juice concentrates prepared by different methods. Freeze preconcentration resulted in the least loss of volatiles as compared to other techniques.

Table 1. Comparison of the Effects of Freeze Preconcentration and Vacuum Preconcentration on the Refractive Index, Sugar Content, Acid Content, Ascorbic Acid Content, and Aroma Compounds Content.

Test material	Refractive index		Total sugar (%)	Acid content		Ascorbic acid mg/100 g	Aroma mg/100 g
	Liquid phase	Solid phase		Liquid phase	Solid phase		
Initial juice	14.0	-[a]	9.24	3.72	-	169.8	13.2
Freeze concentrated	61.2	1.5	31.23	13.00	0.26	596.2	21.36
Vacuum concentrated	76.0	-	38.7	10.64	-	493.8	2.08

Adapted from (4).

[a] Not measured.

Table 2. Average Losses of Volatiles from Fruit Juice Concentrates Prepared by Five Different Methods.

Juice	Volatile loss (%)[a]					Mean
	Freeze	Diffusion membrane	Osmosis	Reverse osmosis	Foam mat powder	
Apple	39	92	88	84	94	79[b]
Cherry	31	42	56	74	63	53
Peach	-[c]	44	65	73	80	66

Adapted from (5).

[a] Measured changes in all peaks that were large enough to integrate.

[b] Statistically significant at 5% level.

[c] Not measured.

b. With adequate remelting and recrystallization, the extent of preconcentration can be chosen.

c. Aromas are retained in the food liquids, thus undesirable polymerization and condensation reactions of the aroma compounds, which may occur in distillation, are fairly well inhibited.

Freeze preconcentration also has its drawbacks, which are given below:

a. Energy consumption is higher compared to newer processes such as reverse osmosis.

b. Capital investment is higher compared to vacuum evaporation. Table 3 summarizes the cost comparisons for preconcentration of a liquid from 10% to 25% solids for several methods as listed by Thijssen (6). The cost of preconcentration using a reverse osmosis process with a capacity for water removal of 46 L/m^2/day (~ 1000 kg/220 days) is almost half that of freeze preconcentration, while capital costs for a typical freeze concentration plant are about double that of an evaporation process.

c. For most liquids, preconcentration cannot be carried out much above the 50-55% solids (about 4- to 5-fold preconcentration by weight for juices) level due to high viscosity which retards the rate of crystallization, hampers the washing of the

Table 3. Concentration Costs per 1,000 kg of Water Removed for Various Processes Operated for 60 and 220 Days.

Process	Specification	$/1000 kg Water	
		60 days	220 days
Two stage long tube evaporator with rectification tower	Capital costs + maintenance	4.91	1.50
	Utilities	4.96	4.96
	Total	9.67	6.46
Centrifugal film evaporator with rectification tower	Capital costs + maintenance	7.03	2.16
	Utilities	5.61	5.61
	Total	12.64	7.77
Reverse osmosis (167 L/m^2/day)	Capital costs + maintenance	8.50	2.32
	Utilities	0.11	0.11
	Total	8.61	2.43
Reverse osmosis (84 L/m^2/day)	Capital costs + maintenance	17.00	4.62
	Utilities	0.11	0.11
	Total	17.11	4.73
Freeze concentration	Capital costs + maintenance	8.07	2.49
	Utilities	2.73	2.73
	Total	10.80	5.22

Adapted from (6).

crystals, and presents difficulties in the separation of ice crystals from the mother liquor.

d. There is always some loss of solids by entrapment in the ice crystals.

Comparison of the Freeze Preconcentration and the Freeze Drying Techniques

The freeze preconcentration process is sometimes confused with the freeze drying technique. A comparison of these two methods is given in Table 4. In freeze drying, water is first frozen as ice in the material, then removed as vapor under vacuum conditions by sublimation. The freeze preconcentration process does not yield a dry product and is considerably less expensive than freeze drying on a per pound of water removal basis. Freeze concentration followed by freeze drying is, therefore, an economically attractive method of producing a quality dry powdered product from an aqueous liquid.

Ney and Martin (7) indicated that freeze drying of sunfish prior to sample preparation could depress metal (Zn, Cd, Pb) concentrations in both the tissue and the whole fish. Maher (8) also mentioned that significant losses of Cr occurred during lyophilization (freeze drying) of selected macroalgae and marine flesh tissues. Powrie (9) studied chemical changes occurring during storage of frozen food. He claimed that chemical changes in frozen foods during storage included protein insolubilization,

Table 4. Comparison of Freeze Preconcentration and Freeze Drying Processes.

	Freeze preconcentration	Freeze drying
Materials to which applicable:	aqueous liquids	aqueous liquids or solids
Form of product when processing completed:	concentrated liquid	dry solid
Basic process involved:	ice crystallization, followed by separation	ice crystallization, followed by sublimation
Water separated from foodstuff in form of:	ice crystals	water vapor
Pressure at which process is performed:	above atmospheric	at high vacuum
Temperature at which process is performed:	slightly below freezing point of solution but above eutectic point	below eutectic point of solution
Amount of volatiles lost:	essentially none	small amount

lipid hydrolysis, and oxidation; natural pigment degradation; vitamin deterioration; and brown pigment formation.

Reasons to Use the Freeze Preconcentration Technique in Analytical Atomic Spectrometry

For the analysis of orange juice, the concentration of Pb is very close to the limit of detection. Such low concentrations make the speciation of the Pb compound ($PbHAsO_4$) very difficult by microwave plasma emission spectroscopy, because the sample is vaporized over a long period of time, resulting in a plasma concentration below the detection limit. Therefore, preconcentration of either the orange juice or the digested solution was necessary. Among several preconcentration techniques, the freeze preconcentration process was chosen because samples could be concentrated without changing chemical forms and without loss of volatile substances. Thus a more accurate As to Pb mole ratio could be obtained, and the speciation of $PbHAsO_4$ by simultaneous measurement of As and Pb by microwave plasma emission spectrometry became possible.

Applications in Analytical Chemistry

Although freeze preconcentration is widely used industrially, it has not yet been used routinely by analysts. Moreover, references to its use in analysis are rare. In 1961, Shapiro demonstrated that freeze preconcentration is simple, inexpensive, and does not alter chemical or physical characteristics of the substances being concentrated. The method is applicable to a very wide range of volumes and has been used in his laboratory on samples as small as 100 mL and as large as 300 L (10). No sample data, however, were reported in the paper. Later in 1967, he showed 89.4, 89.7, and 102% recovery of NaCl, $CH_3CH(OH)CH_3$, and CH_3COCH_3, respectively, by concentrating 15 L of distilled water to 3 L (11). A number of researchers have used this technique to concentrate a variety of materials including sodium salts (12), Rhodamine B (13), and gold and mercury (14). Results of these studies are shown in Table 5 with the initial volume, final volume, original solute concentration, recovery, and time required.

All freeze preconcentration runs are terminated when cloudiness appeared around the portions of the core. As discussed by Himes et al. (15), cloudiness is probably due to occlusion. Clear demarcations among solution, clear ice, and salt deposits could be observed by adding small quantities of sodium fluorescein. In solution, this dye emits a green fluorescence. However, when trapped among the ice crystals, it had a characteristic orange-red color. Growth of ingots has been observed, and crystallites were examined by microscopy. Average salt concentrations have been measured by conductivity analysis. This phenomena may occur at a freezing interface, when removal of solute is slow relative to the

Table 5. Application of Freeze Preconcentration Process in Analytical Chemistry.

Analyte (concentration)	Initial volume (mL)	Final volume (mL)	Recovery (%)	Time required (hr)	Ref.
NaCl (10 ppm)	15000	3000	89.4	n	11
$CH_3CH(OH)CH_3$ (50 ppm)	15000	3000	89.7	n	11
CH_3COCH_3 (100 ppm)	15000	3000	102	n	11
NaH_2PO_4 (20 μg)	100	10	94-100	3	12
NaCl (45 μg)	100	10	98-102	3	12
Rhodamine B (75 μg)	2200-5000	223-1325	82-94	n	13
Au (0.03-5.0 μg)	50-400	10	84-97	1.5-5	14
Hg (2 μg)	50-400	10	95-97	1.5-5	14

n: no report data.

rate of advance of the ice-liquid interface (10). The purpose of stirring is, therefore, to minimize the formation of cloudiness. Rates at which clear ice occurs increase with degree of stirring and decrease with increasing solute concentration. Yonehara et al. (16) showed that the ice occluded the solute and became cloudy when the total solute concentration in the remaining solution reached about $4x10^{-2}$ mol/dm^3.

All previous preconcentration procedures have dealt only with deionized water only. The aim of this work is to expand the application solution to tap water and orange juice with or without an acid digesting procedure. Unfortunately in the latter cases, considerable losses of the analyte occurred. These results are discussed in a latter section.

Fundamental Considerations

Principle of the Process

The principles of zone melting and freeze preconcentration are the same. Both are types of fractional crystallization processes. Freeze preconcentration is also called progressive freezing and is superior to zone melting involving a single zone.

Separation by freezing is based on a solid-liquid phase equilibrium. The solution to be concentrated contains a large number of soluble components dissolved in water. However, for all practical purposes, it is considered as a pseudo-binary system (2), where all substances dissolved in water are considered as one component. A simple phase diagram of a binary mixture is shown in Figure 1 (10). When a binary mixture is cooled under conditions allowing equilibrium to be attained, pure ice crystals separate out at a point which corresponds to composition W_A and the freezing point of this solution (T_A'). Further cooling results in more separating out of the ice crystals, while liquid composition follows the line $((W_A,T_A')(W_B,T_B))$, with W_B and T_B as the final concentration and temperature of solution, respectively. At W_E (the eutectic concentration), the crystallizing solid has the same composition as the supernatant liquid. In most cases, because of the problems connected with separating ice from a very concentrated liquid, the solidification process must stop well above the eutectic point.

Simple Engineering Approach

The moving interface problem of freezing a liquid inside a container is important in many engineering applications, such as the freezing of food (17), the formation of polar ice (18), the casting of metals (19,20), welding, and many other operations (21,22). Freezing or melting produces various kinds of geometric shapes. The solid-liquid interface is often irregular and can be oscillatory. The process involves mass transfer from ice

Figure 1. Phase diagram for a simple binary system. W_E, eutectic concentration; T_E, eutectic temperature, T_A, initial temperature of solution; W_A, initial concentration of solution; T_f, freezing point of pure solvent; $T_{A'}$, freezing point of solvent; W_B, final concentration of solution; T_B, final temperature of solution. Adapted from (10).

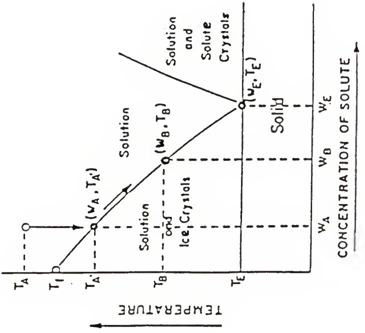
TEMPERATURE
CONCENTRATION OF SOLUTE
T_A
T_I
T_A'
T_B
T_E
w_A
w_B
w_E
(w_A, T_A')
(w_B, T_B)
(w_E, T_E)
Solution
Solution and Ice Crystals
Solution and Solute Crystals
Solid

to liquid and heat transfer from liquid-ice interface through the ice, the ice-container interface, and the container to coolant. The development of a mathematical model to describe solidification of cylinders is complicated by a number of factors. One of the most problematic of these is the difficulty of simultaneous treatment of heat flow through the ice and container by thermal conduction and across the ice-container interface by Newtonian heat transfer. The most idealized and generalized solutions were made by London and Seban (18) and Tao (23). The former used an approximate method and the latter used a numerical method which included the solution of Laplace equations. The intention of these developments is to predict the position of the solid-liquid interface at any time as a function of the physical and geometric properties of the system. These two methods arrived at the same result. The solution has been modified for application to other similar systems, such as metal solidification (24) and a cooled cylinder in water crossflow (25).

The basic assumptions of all these models, which are similar when treating the solidification problem, are given below:

a. Heat flow is geometrically unidimensional.

b. Newtonian interface resistance remains constant throughout the process.

c. Thermal properties are independent of both position and time.

d. Volume changes due to liquid and solid densities are neglected.

e. Solidification occurs between the two constant temperatures of liquid and coolant.

Figure 2 shows the temperature distribution of real and virtual systems during solidification in a cooled container. The generalized solution is based upon the virtual coordinate system, which is displaced from the real coordinate origin by the thickness of virtual adjunct introduced, as illustrated in Figure 2. The equations below were derived by London and Seban (18). Figure 3 shows the system and the thermal equivalent circuit. In the system, ice forms in the direction of decreasing radius within a cylinder. The thermal current flows through the ice by conduction and the ice-container interface by convection. The ice resistance R_i for a unit length of the cylinder is given by

$$R_i = (\log r_o/r)/2\pi k \ (\mathrm{s\ cm\ {}^oC\ cal^{-1}}) \tag{1}$$

and the surface resistance R_o is given by

$$R_o = 1/2\pi r_o h_o \ (\mathrm{s\ cm\ {}^oC\ cal^{-1}}) \tag{2}$$

The physical meaning of symbols used in equations are listed in Table 6.

Figure 2. Real ice/container system during the solidification in cooled container (full line) and correspondent virtual system (dashed line). T_o, temperature of the coolant; T_i, surface temperature; T_s, temperature at any point in the solidified ice; T_f, freezing temperature of ice; S, thickness of solidifed ice; S_o, thickness of container. Adapted from (24).

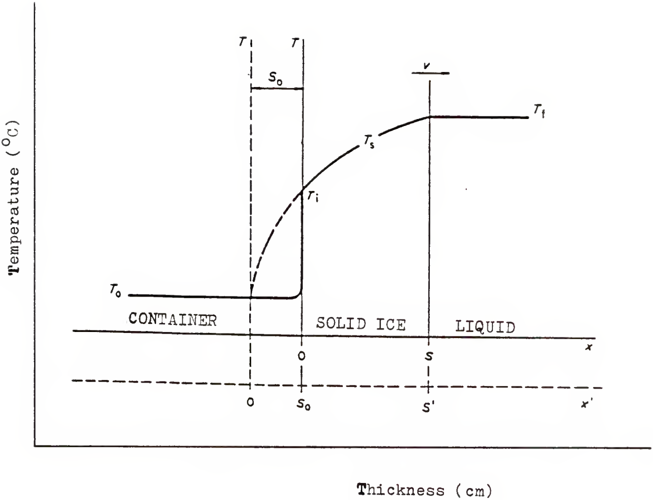
T
T
S₀
v
T_f
T_s
T_i
T₀
CONTAINER
SOLID ICE
LIQUID
0
S
x
0
S₀
S'
x'
Temperature (°C)
Thickness (cm)

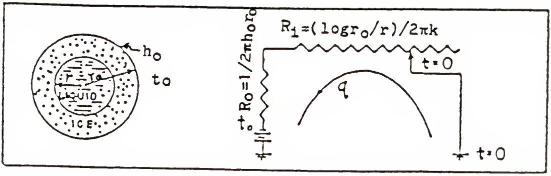

Figure 3. Cylindrical-ice formation $r^* \leq 1$ and thermal-circuit representation.

Table 6. Physical Meaning of Equation Parameters.

Equation Parameter	Meaning
h_o	unit conductance to surroundings at temperature t_o (cal cm^{-2} s^{-1} $^oC^{-1}$)
k	unit thermal conductivity of ice (cal cm^{-1} s^{-1} $^oC^{-1}$)
L	latent heat of fusion of ice (cal g^{-1})
q	thermal current (cal cm^{-2} s^{-1})
r_o	radius of cylinder (cm)
r	radial position of growing ice surface (cm)
R	unit thermal resistance (s cm ^oC cal^{-1})
t_o	temperature of surroundings (^oC)
ρ	ice density (g cm^{-2})
τ	time (s)
r*	r/r_o, generalized radial position
R*	h_or_o/k, generalized surface resistance
τ*	$(-t_ok/\rho Lr_o^2)\tau$, generalized time

The rate equation for the thermal current q (cal s^{-1} cm^{-1}) flowing through the resistances offered by the ice and the surface, acting in series, as a result of the temperature drop $-t_o$ is

$$q = -t_o/(R_i + R_o) \tag{3}$$

The thermal current q provides for the extraction of the latent heat of fusion necessary for freezing at the surface r:

$$q = -2\pi\rho Lr\frac{dr}{d\tau} \tag{4}$$

where $-2\pi r\frac{dr}{dt}$ is the volume rate of ice formation at the growing surface, cm^3 s^{-1} cm^{-1}, and ρL, the latent heat of fusion, cal $cm^{3^{-1}}$.

Combination of Equations 3 and 4 to eliminate the thermal current q provides the differential equation expressing radius r as a function of time t:

$$-2\pi\rho Lr\frac{dr}{d\tau} = -t_o/(\frac{\log\frac{r_o}{r}}{2\pi k} + \frac{1}{2\pi r_o h_o}) \tag{5}$$

This equation may be readily rearranged in the following dimensionless form, employing the generalized radius r*, resistance R*, and time τ*:

$$(-\log r^* + \frac{1}{R^*})\ r^*dr^* = -d\tau^* \tag{6}$$

The boundary conditions are

$$r = 0,\ r^* = 0,\ r = r_o,\ r^* = 1 \tag{7}$$

For these conditions, the solution of Equation 6 becomes

$$\tau^* = \frac{r^{*2}}{2}\log r^* + (\frac{1}{2R^*} + \frac{1}{4})(1 - r^*) \tag{8}$$

$$\tau^* = f(r^*, R^*)$$

The time for complete solidification ($r^* = 0$), which can be determined from Equation 8 and is

$$\tau^*_{r^*=0} = (\frac{1}{2R^*} + \frac{1}{4}) \tag{9}$$

An example of the use of the above equations will be given in the section on results and discussion.

Experimental Section

Apparatus

Freeze preconcentration system. The freeze concentration apparatus is shown in Figure 4. Suitable subtances were chosen as the coolant, for instance,

Figure 4. Cross-sectional view of freeze preconcentration system.

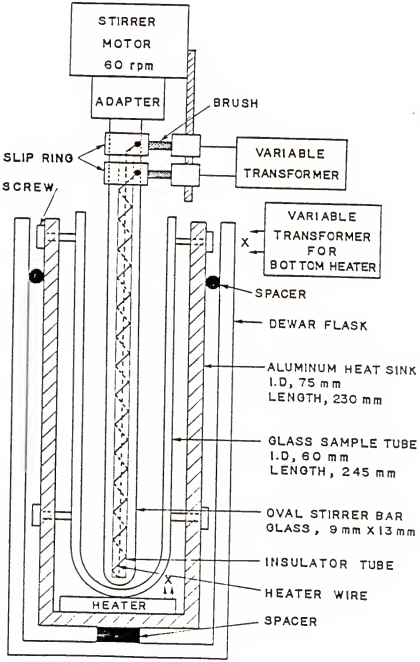
STIRRER MOTOR 60 rpm
ADAPTER
BRUSH
SLIP RING
SCREW
VARIABLE TRANSFORMER
VARIABLE TRANSFORMER FOR BOTTOM HEATER
X
SPACER
DEWAR FLASK
ALUMINUM HEAT SINK I.D, 75 mm LENGTH, 230 mm
GLASS SAMPLE TUBE I.D, 60 mm LENGTH, 245 mm
OVAL STIRRER BAR GLASS, 9 mm X 13 mm
INSULATOR TUBE
HEATER WIRE
X
HEATER
SPACER

NaCl/ice (-21.3°C) and liquid N_2 (-196°C) were used in our experiments. Sample glass tubes of two different sizes could be selected: the small one (I.D. 40 mm, depth 150 mm) for 100 mL of sample solution and the large one (I.D. 60 mm, depth 250 mm) for 500 mL of solution. The central glass heater and bottom heater were controlled separately by two variable transformers. The central glass heater was attached to a motor stirrer (60 rpm). The purpose of the screws was to prevent direct contact of the glass sample tube with the aluminum heat sink; otherwise, nonuniform ice would result. Three pieces of rubber tubing were used as spacers.

Graphite furnace atomic absorption spectrometry (GFAAS). A Hitachi Model 180-80 atomic absorption spectrometer equipped with a 3 cm graphite tube furnace atomizer was used to measure the concentrations of As and Pb, with As and Pb hollow cathode lamps (Hamamatsu). The cuvette atomizer was made of graphite and consisted of either the cup type or the tube type. The former type was used especially for metals of low melting point (Pb, for example) because the temperature of the cup section lagged behind the temperature of both cuvette ends, thus reducing analyte loss due to vaporization of volatile samples. A static magnetic field of 10 kG was applied to the graphite atomizer, and differential absorption was observed for radiation polarized perpendicular and parallel to the magnetic field, respectively.

The signal from the photomultiplier was processed by a microprocessor after A/D (analog/digital) conversion by a V/F (voltage/frequency) converter. Analytical results were shown on a character display and hard copied by a printer. The operating characteristics of the instrument are shown in Table 7.

Evolved gas analysis/single electrode microwave plasma emission spectrometry (EGA/SEMPES). A single electrode atmosphere pressure helium microwave plasma was used for the identification of $PbHAsO_4$ and $C_2H_4Br_2$, to ensure the simultaneous measurement of Pb and As, Br and H, or Br and C is possible. This plasma had been modified and improved by Hanamura et al. (26-28). Figures 5 and 6 show the block diagram of the EGA/SEMPES system and the schematic diagram of the plasma torch. Compared to other single electrode microwave plasma systems, this plasma torch has a special platinum-clad electrode, which minimizes wear of the plasma-support electrode and elemental contamination and maximizes stability.

The sample vaporization furnaces are shown schematically in Figures 7 and 8. The temperature of the induction furnace (Figure 7) reached ~ 1800°C, and the electric resistance heater (Figure 8) reached ~ 500°C. The sample was held in a quartz crucible, and as the sample was

Table 7. Instrument Settings of Graphite Furnace Atomic Absorption Spectrometer.

	As	Pb
drying time	30 s	30 s
drying temperature	120°C	120°C
ashing time	30 s	30 s
ashing temperature	400°C	400°C
atomization time	7 s	7 s
atomization temperature	2800°C	2000°C
cleaning temperature	2800°C	2800°C
wavelength	193.7 nm	283.3 nm
slit width	2.6 nm	1.3 nm
cuvette	tube	cup
argon flow	0.2 L/min	0.2 L/min
magnetic field strength	10 kG	10 kG

Figure 5. Block diagram of Evolved Gas Analysis/Single Electrode Microwave Plasma Emission Spectrometer (EGA/SEMPES).

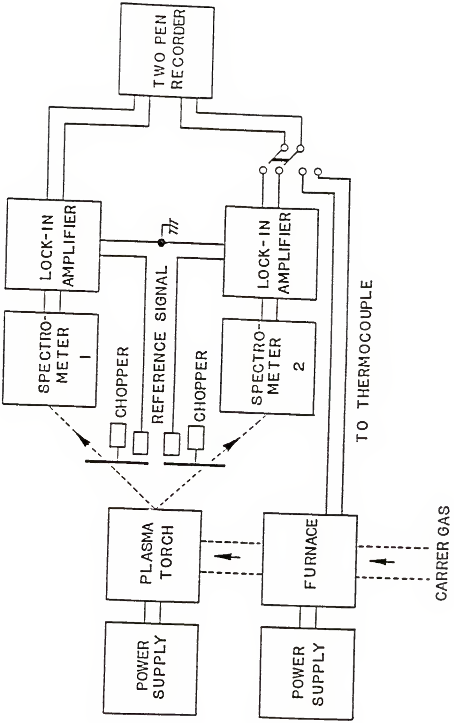
TWO PEN RECORDER
LOCK-IN AMPLIFIER
LOCK-IN AMPLIFIER
SPECTRO-METER 1
SPECTRO-METER 2
CHOPPER
REFERENCE SIGNAL
CHOPPER
TO THERMOCOUPLE
PLASMA TORCH
FURNACE
CARRER GAS
POWER SUPPLY
POWER SUPPLY

Figure 6. Schematic diagram of the single electrode microwave plasma torch.

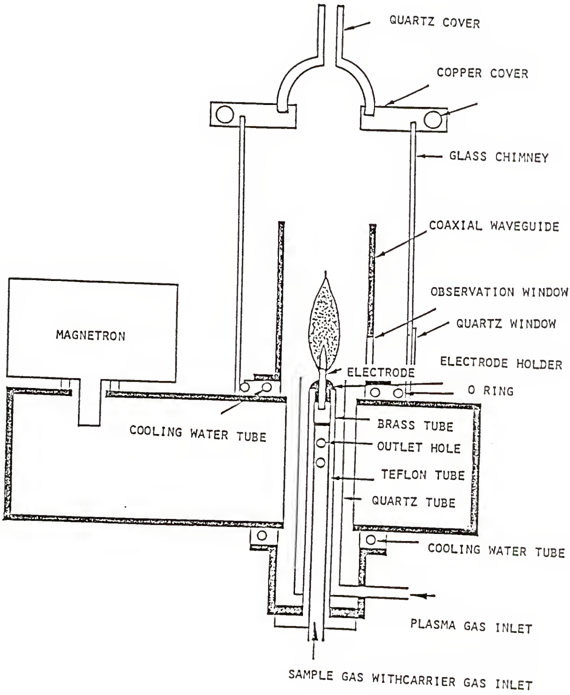
QUARTZ COVER
COPPER COVER
GLASS CHIMNEY
COAXIAL WAVEGUIDE
OBSERVATION WINDOW
QUARTZ WINDOW
MAGNETRON
ELECTRODE HOLDER
ELECTRODE
O RING
BRASS TUBE
COOLING WATER TUBE
OUTLET HOLE
TEFLON TUBE
QUARTZ TUBE
COOLING WATER TUBE
PLASMA GAS INLET
SAMPLE GAS WITHCARRIER GAS INLET

Figure 7. Schematic diagram of induction furnace vaporization system.

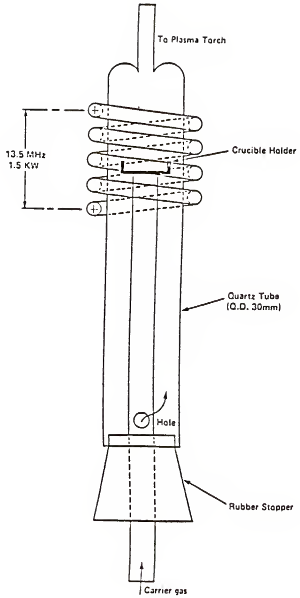
To Plasma Torch
13.5 MHz
1.5 KW
Crucible Holder
Quartz Tube
(O.D. 30mm)
Hole
Rubber Stopper
Carrier gas

Figure 8. Schematic diagram of electric resistance furnace vaporization system.

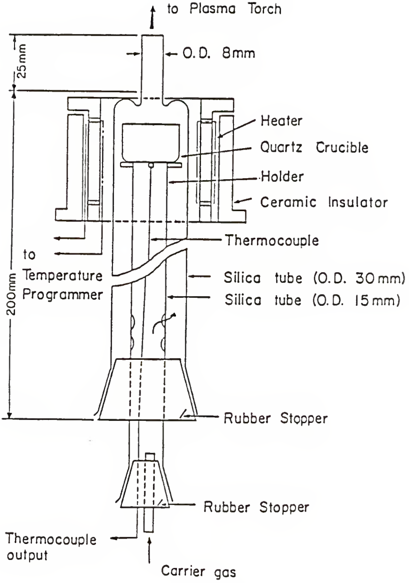
to Plasma Torch
O.D. 8mm
25mm
Heater
Quartz Crucible
Holder
Ceramic Insulator
Thermocouple
to
Temperature
Programmer
200mm
Silica tube (O.D. 30mm)
Silica tube (O.D. 15mm)
Rubber Stopper
Rubber Stopper
Thermocouple
output
Carrier gas

heated, the volatile constituents were swept by the carrier gas into the plasma. The temperature of the induction furnace was measured by an optical pyrometer, while an alumel-chromel thermocouple (BTS gauge 28) was used to monitor the temperature of the resistance furnace. The temperature of the resistance furnace, which was increased at a certain rate, was adjusted by a 250 W heating coil controlled by a linear temperature programming unit taken from a commercial gas chromatograph (Varian, Palo Alto, CA).

Reagents

All standard solutions were prepared by dissolution of standard materials in acid and diluted to the appropriate volumes.

A 20 ppm $PbHAsO_4$ solution was prepared by dissolution of 0.0100 g $PbHAsO_4$ (C.P. grade, Baker & Adamson) in 500 ml deionized water. A 1.09×10^{-3} ppm $C_2H_4Br_2$ solution was prepared by dissolution of 0.500 mL (±0.005 mL) $C_2H_4Br_2$ (density = 1.5379 g/mL, A.C.S. grade, Fisher Scientific) in 1000 mL deionized water. High purity HNO_3 was prepared by distillation at subboiling temperature.

Procedures

The aluminum heat sink and sample glass tube were properly aligned, the coolant was poured into the dewar flask carefully, and the system was then allowed to reach a constant temperature. Finally, sample solution was placed in the sample glass tube after the central and bottom heaters had been turned on and adjusted to the optimum voltages. Several voltages were tested; those with the formation of uniform ice crystals was chosen as the optimum voltage (40 V and 20 V for the central and the bottom heaters, respectively). When the NaCl/ice mixture was used as the coolant, no heater was needed, and teflon stirring bar was attached to the motor stirrer instead. The motor stirrer was used to gently stir the solution.

The first experiment involved preconcentration of 100 mL deionized water containing 0.2 ppm $PbHAsO_4$, to a final volume of 25 mL. The second experiment was done on 500 mL of deionized water or tap water to which 1 mL of 20 ppm $PbHAsO_4$ or 1 mL of 40 ppm $C_2H_4Br_2$ had been added. After 2-3 hours of freezing, most of the solution was frozen except for the central part of the tube, which contained the concentrated solutes. The final volume was 25 mL for every experiment. The preconcentration factor was 4 X for the first experiment and 20 X for the second experiment. Each experiment was repeated several times for the calculation of average recovery.

The concentration of As and Pb were then determined by graphite atomic absorption spectroscopy (GFAAS). The concentration of $C_2H_4Br_2$ along with the speciation investigations of As and Pb in $PbHAsO_4$, and Br and H (or C) in $C_2H_4Br_2$ were consequently determined by EGA/SEMPES.

Results and Discussion

Recovery of As and Pb

The results of the first experiment with the NaCl/ice freeze mixture, in which no heater was needed, are given in Table 8. The concentration factor was 4 X and recovery was 97% for both As and Pb with no HNO_3 in the solution. For solutions with 0.015 M HNO_3, the recoveries were decreased slightly to 88% and 90% for As and Pb, respectively.

The effect of different volume of saturated HNO_3 (0.05 mL, 0.1 mL, 0.2 mL, 0.3 mL) added into the 100 mL initial solution was evaluated. Only the solutions with $\leq$ 0.1 mL HNO_3 (concentration $\leq 1.5\times10^{-2}$ M) produced clear ice, while the others with higher HNO_3 concentrations yielded cloudy ice, which implied solute losses by entrapment.

The critical HNO_3 concentration (from 1.5×10^{-2} M to 6.0×10^{-2} M) agreed quite well with the results by Yonehara et al. (16). They concluded that ice would start to occlude the solute and become cloudy when total solute concentration (HNO_3 + analytes) in the remaining solution reached about 4×10^{-2} M.

Table 9 shows the recovery of $PbAsH_4$ in deionized and tap water when liquid N_2 was used as the coolant and both heaters were used. The preconcentration factor was 20 X, and the recoveries of $PbAsH_4$ in deionized were 77% and 81% for As and Pb, respectively. The time to accomplish the

Table 8. Recovery* of Lead Arsenate from Deionized Water with 4-Fold Freeze Preconcentration.

Sample	Pb	As
a	98%	91%
b	98%	93%
c	96%	99%
d	96%	103%
	$\bar{x}$ = 97%	$\bar{x}$ = 97%
e	89%	100%
f	89%	89%
g	90%	81%
h	90%	75%
	$\bar{x}$ = 90%	$\bar{x}$ = 86%

* Original solution--100 ml of 0.2 ppm $PbHAsO_4$ solution; final solution volume--25 ml; coolant ice and NaCl mixture, -22°C; sample a, b, c and d contained no HNO_3 and sample e, f, g and h contained about 0.015 M HNO_3.

Table 9. Recovery* of Lead Arsenate from Deionized and Tap Water with 20-Fold Freeze Preconcentration.

Sample	Pb	As
a	81%	83%
b	82%	73%
c	81%	76%
	$\bar{x}$ = 81%	$\bar{x}$ = 77%
d	17%	13%
e	16%	19%
	$\bar{x}$ = 17%	$\bar{x}$ = 16%

* Original solution--500 ml of 0.03 ppm $PbHAsO_4$ solution; final solution volume--25 ml; coolant-liquid nitrogen, -196°C; sample a, b and c--deionized water solution; and sample d and e--tap water solution.

freeze preconcentration of 20 X was around 3 hr. The lower recovery of $PbHAsO_4$ in deionized water was due to the ice entrapment because somewhat cloudy ice which entrapped the analyte could be observed (15). The recoveries could be increased if more time was used to accomplish the preconcentration process, which would mean more power would be consumed.

The recovery using liquid nitrogen coolant (see Table 9) was lower for $PbHAsO_4$ in tap water, based upon the work of others (16), this suggested the total solute concentration was much higher than 6.0×10^{-2} M. The tap water was also freeze preconcentrated by using NaCl/ice freeze mixture as coolant, where the rate of ice formation was slower and diffusion of solute could be more complete, but cloudy ice still occurred and the results would be even poorer than in Table 9.

The recoveries of As were more scattered than those of Pb, but the average value of As was similar to the recoveries of Pb. This suggested that $PbHAsO_4$ diffused as a molecular species which will be further verified by the speciation study. The fluctuation of As recoveries might be due to the graphite furnace measurements, where reactions occurred on the graphite surface and the stability of As hollow cathode lamp was poor.

Concentrated orange juice, which already had been freeze concentrated 4 X by an industrial process, was concentrated additionally in our laboratory by NaCl/ice and liquid N_2. However, it was not possible to separate the ice from the liquid phase. The purpose of expanding the freeze preconcentration technique to tap water and orange ice is, therefore, not a viable analytical tool for real samples.

Although the recovery decreased slightly, when liquid N_2 and heaters were used in the freezing system instead of the NaCl/ice freeze mixture, the concentration factor was 5 X higher, and the freezing time was only increased from 2 hr to 3 hr.

When applying Equation 8 to our freezing system, the following physicochemical quantities were used:

$k = 5.3 \times 10^{-3}$ cal cm^{-1} s^{-1} $^{o}C^{-1}$, unit therml conductivity of ice;

$\rho = 0.91$ g ml^{-1}, ice density;

$L = 79.8$ cal g^{-1}, latent heat of fusion of ice; and

$ho = 0.61$ cal cm^{-2} s^{-1} $^{o}C^{-1}$, unit conductance to surroundings.

The time calculated to be needed to complete the first experiment ($r = 6$ mm, $r_o = 20$ mm) is about 10 min and is about 2 min to accomplish the second experiment ($r = 6$ mm, $r_o = 28$ mm). The exact time required to finish the first and the second experiments in our laboratory was 3 hr and

2 hr, respectively. Reasons for the time difference are (1) the unit thermal conductivity of ice is very small (k = 5.3×10^{-3} cal cm^{-1} s^{-1} $^oC^{-1}$), for example, the time to cool 100 mL of water from 25°C to 0°C is 1 cal g^{-1} $^oC^{-1}$ x 100 g x 25°C = 5.3×10^{-3} cal cm^{-1} s^{-1} $^oC^{-1}$ x 2 cm (ice radius) x 22°C (NaCl/ice coolant) x t and t ≃ 10^4 s ≃ 3 hr; (2) an initial sample solution temperature of 0°C was assumed in calculations with Equation 8, while the initial temperature of the real sample solutions was room temperature, more time was, therefore, needed to transfer the extra heat content of the water to the coolant; and (3) a certain amount of power was supplied through the transformers to the central and bottom heaters in the second experiment (heaters were not used in the first experiment), thus more and more time was required to obtain the phase steady state. The experimental time to freeze the total water in the second experiment without heaters was 5-6 min, but cloudy ice occurred in the whole sample tube; this time is near the calculated time. With sample solution at an initial 25°C temperature (room temperature) and heaters (only in the second experiment), sample solutions were allowed to freeze concentrate slowly, and the diffusion of analytes into the liquid phase would be more complete. Equation 8 can only be used to estimate the time required to crystallize the total sample solution when the initial

temperature of sample solution was at 0^oC and no heaters were attached.

Speciation of $PbHAsO_4$

The important factors for the identification of species by EGA/SEMPES are (1) initial evolution temperature; (2) peak temperature, in the intensity vs temperature curve; and (3) mole ratio of elements which exist in the molecular form. In the case of $PbHAsO_4$, the sample was placed first in the quartz crucible and then into the induction furnace. Figures 9, 10, and 11 show the emission intensity vs evolution temperature profiles for O and Pb, H and Pb, and As and Pb, respectively. These measurements were run separately, the traces of the same element differ slightly due to statistical and systematic errors associated with transfer of the samples to furnace and transport of the vapors to the plasma.

Lead arsenate at about 280^oC loses H_2O and is converted into $Pb_2As_2O_7$, which has a m.p. of 802^oC. Peak a in Figure 9 is due to oxygen which resulted from a room air leak during the sample insertion. Peak b in Figure 9 and peak c in Figure 10 are oxygen and hydrogen peaks that appeared at the same evolution temperature. These presumably correspond to water loss. Peaks for As and Pb in Figure 11 appeared at the same evolution temperature, and so it suggests that the sample of $PbHAsO_4$ preconcentrated and evaporated with no change in chemical

Figure 9. Evolution temperature profiles for Pb and O from $PbHAsO_4$; peak a--O from air leak; peak b--O from H_2O loss. Experimental conditions: microwave power = 500 W; wavelengths, O = 777.1 nm and Pb = 405.7 nm; broken line, sample furnace temperature.

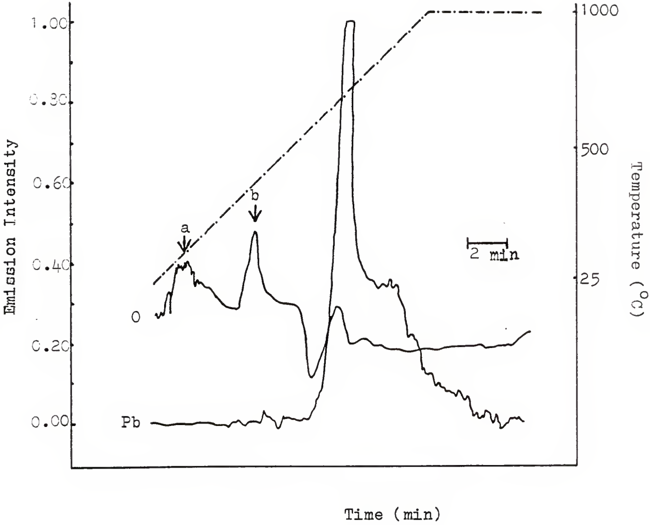
1.00
0.80
0.60
0.40
0.20
0.00
Emission Intensity
O
Pb
a
b
2 min
1000
500
25
Temperature (°C)
Time (min)

Figure 10. Evolution temperature profiles for Pb and H from $PbHAsO_4$; peak c--H_2 from H_2O loss. Experimental conditions: microwave power = 500 W; wavelengths, H = 656.2 nm and Pb = 405.7 nm; broken line, sample furnace temperature.

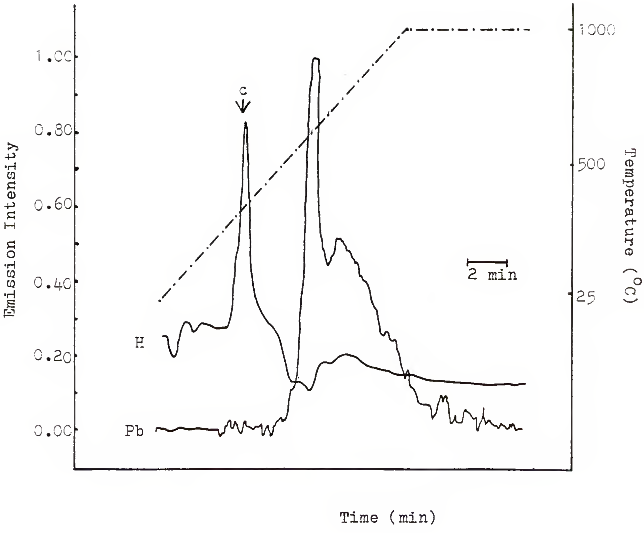
Emission Intensity
1.00
0.80
0.60
0.40
0.20
0.00
c
H
Pb
2 min
1000
500
25
Temperature (°C)
Time (min)

Figure 11. Evolution temperature profiles for Pb and As from $PbHAsO_4$. Experimental conditions: microwave power = 500 W; wavelengths, Pb = 405.7 nm and As = 197.2 nm; broken line, sample furnace temperature.

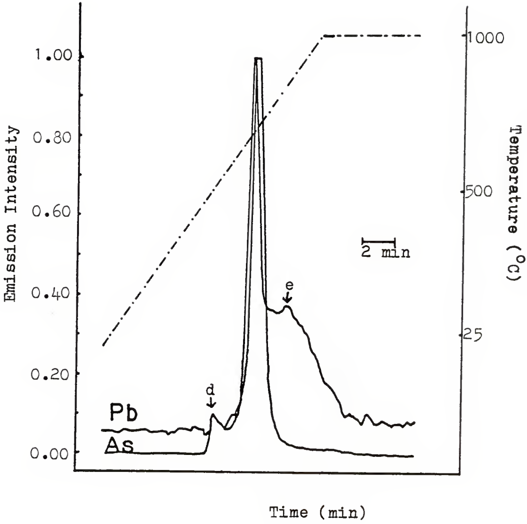
1.00
0.80
0.60
0.40
0.20
0.00
Emission Intensity
1000
500
25
Temperature (°C)
2 min
d
e
Pb
As
Time (min)

form. As shown in the literature (29), $Pb_2As_2O_7$ is a stable compound and decomposition before melting point does not occur; these facts make the explanation of peak d and e extremely difficult. If peak d was due to the vaporization of a arsenic compound (As_2O_3, As_2O_5 or AsH_3) and peak e was due to the vaporization of a lead compound (PbO), signals of O or H should have been observed at the same temperature. Since there are no peaks of O or H, the only reasonable sources for these two peaks are due to the vaporization of metallic As and Pb. However, these explanations need further proof.

Recovery of $C_2H_4Br_2$

Ethylene dibromide is used primarily as an additive in leaded gasoline; relatively small quantities are used as pesticides in soil fumigants and in grain and commodity fumigants. The accepted concentration of C_2H_4Br in drinking water, which was regulated by EPA (U.S. Environmental Protection Agency), is 0.02 ppb. A purge-and-trap sampling system (EPA method 624) was used to isolate $C_2H_4Br_2$ from the water samples, and a GC/MS spectrometer was used to determine the $C_2H_4Br_2$ concentration (30). The limit of detection of GC/MS spectrometry is 0.1 ppb, which implies that the preconcentration factor by the purge-and-trap sampling system is higher than 5 X.

Figure 12 shows microwave plasma emission spectra (400-900 nm) for $C_2H_4Br_2$ solution with and without water in our laboratory. According to Hanamura et al. (31), the plasma temperature drops 400°K (from 7050°K to 6650°K) when water vapor was present in the He plasma and the microwave input power was 500 W.

Table 10 shows the emission intensity ratio of four selected Br emission lines ($I_{C_2H_4Br_2+H_2O}/I_{C_2H_4Br_2}$); these four lines were selected from the table of Br line spectra in the literature (32). Symbol I represents neutral atom lines and II singly ionized lines. The Br atom line I 827.246 nm was chosen as the Br emission wavelength, because it had the highest intensity when there was water vapor in the He plasma.

Figure 13 shows the analytical calibration curve of $C_2H_4Br_2$. Bromine emission signals were determined by microwave plasma emission spectrometry. Different concentrations of $C_2H_4Br_2$ solutions were prepared by dilution of the original 1.09×10^3 ppm $C_2H_4Br_2$ solution. Figure 14 shows a comparison of the Br signal level of $C_2H_4Br_2$ in the original tap water solution, the first melting ice solution (400 mL, from 500 mL to 100 mL), the second melting ice solution (75 mL, from 100 mL to 25 mL), and the final volume solution (25 mL). $C_2H_4Br_2$ concentration in the final solution is definitely higher than in the original solution, but the ratio is far less

Figure 12. Emission spectra (400-900 nm) of $C_2H_4Br_2$ in single electrode microwave plasma. Experimental conditions: sample 1, $C_2H_4Br_2$ solution; sample 2, $C_2H_4Br_2$ solution with water. Identical wavelengths are a, II 470,4 nm; b, II 478.5 nm; c, II 481.6 nm; d, I 827.2 nm.

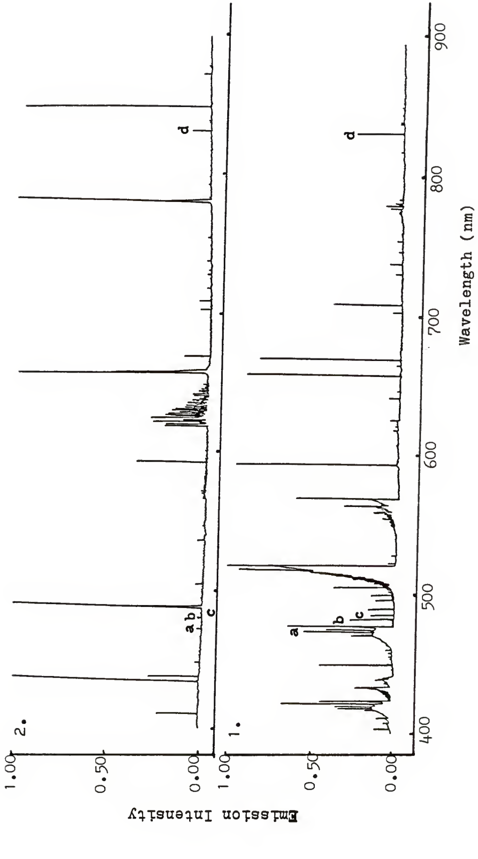
2.
1.
1.00
0.50
0.00
1.00
0.50
0.00
Emission Intensity
a
b
c
d
a
b
c
d
400
500
600
700
800
900
Wavelength (nm)

Table 10. Comparisons of Emission Intensities of Four Bromine Emission Lines for $C_2H_4Br_2$ in the Single Electrode Microwave Plasma.

Wavelength (nm)	I_1 (relative unit)[a]	I_2 (relative unit)	I_2/I_1
I 827.246	1.4	0.50	0.36
II 481.671	0.7	0.07	0.10
II 478.550	1.3	0.10	0.077
II 470.480	3.7	0.15	0.040

I: atom line, II: ion line.

I_1: $C_2H_4Br_2$ alone, I_2: $C_2H_4Br_2$ with water vapor.

[a] Relative peak height length on the recording paper.

Figure 13. Microwave emission analytical calibration curve of $C_2H_4Br_2$ introduced into single electrode microwave plasma. Experimental conditions: microwave power = 500 W; wavelength, Br = 827.2 nm.

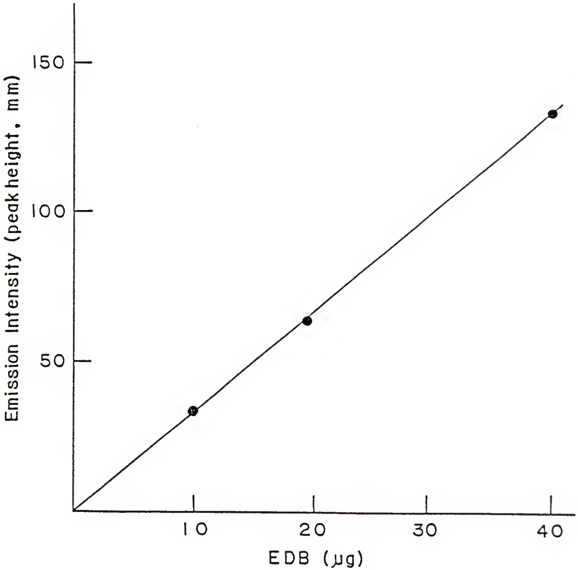
Emission Intensity (peak height, mm)
150
100
50
10
20
30
40
EDB (μg)

Figure 14. Comparison of Br emission signals for $C_2H_4Br_2$ in several different solutions. Legend: a, original tap water solution; b, first ice solution; c, second ice solution; d, final solution. Experimental conditions: microwave power = 500 W; Br emission wavelength = 827.2 nm.

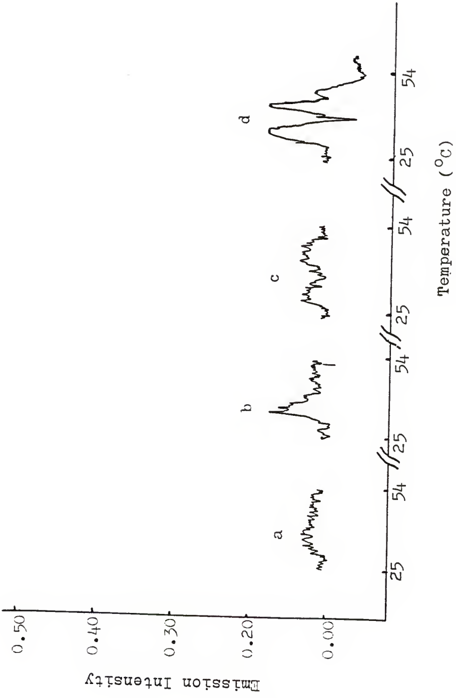
Emission Intensity
0.50
0.40
0.30
0.20
0.00
Temperature (°C)
25
54
25
54
25
54
25
54
a
b
c
d

than 20 X (from 500 mL to 25 mL). Entrapment losses in the ice could explain part of the loss. In addition, during the freeze concentration process, an appreciable quantity of $C_2H_4Br_2$ escaped from the sample solution because of the stirring system; this is discussed in the next paragraph.

Figure 15 shows $C_2H_4Br_2$ (in tap water) loss due to stirring and with air blowing above the solution surface (hood suction) at room temperature condition. Both cases indicate that $C_2H_4Br_2$ would be completely lost (not detectable) after 6 hr; curves b and c are the same as background (tap water) signal, in which trace of carbon exists in the tap water.

Figure 16 shows the loss in $C_2H_4Br_2$ (in tap water) at 15 min intervals, while the solution was stirred. Signal of $C_2H_4Br_2$ disappeared after 45 min. The background signals (see Figure 16) depended on the amount of sample and the conditions of the detecting devices, and sometimes they are hard to define. The decay curve is shown in Figure 17. Shapiro (10) had a similar report, in which iodine solution (12.7 ppm in 15 L deionized water), which was exposed to air and was stirred at room temperature, lost all the signal within a certain period of time (no data were reported).

Results of the $C_2H_4Br_2$ preconcentration were not reproducible, but signals always appeared when the sample

Figure 15. Comparison of Br emission signals for $C_2H_4Br_2$ for several different conditions.

Legend: a, freshly prepared solution; b, after 6 hr stirring; c, after 6 hr in the hood. Experimental conditions: microwave power = 500 W; emission wavelengths, C = 247.8 nm and Br = 827.2 nm.

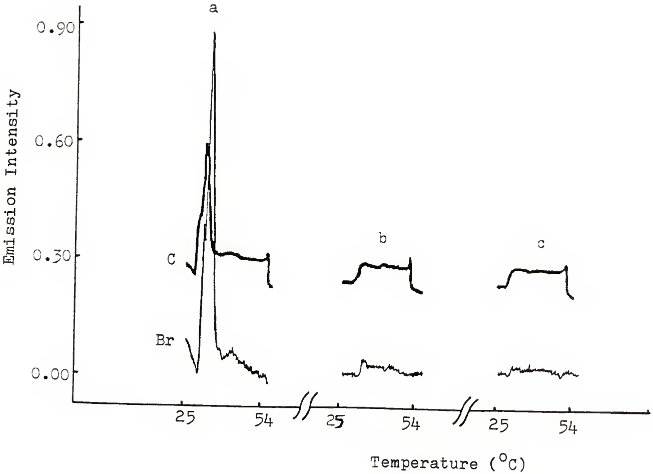
a
b
c
C
Br
Emission Intensity
0.90
0.60
0.30
0.00
25
54
25
54
25
54
Temperature (°C)

Figure 16. Comparison of loss of $C_2H_4Br_2$ at 15 min stirring intervals. Legend: a, fresh prepared solution; b, after 15 min stirring; c, after 30 min stirring; d, after 60 min stirring; e, tap water (no $C_2H_4Br_2$). Experimental conditions: microwave power = 500 W; emission wavelengths, C = 247.8 nm and Br = 827.2 nm; recorder, 0.5 mV full scale for a and 0.2 mV for b, c, d and e.

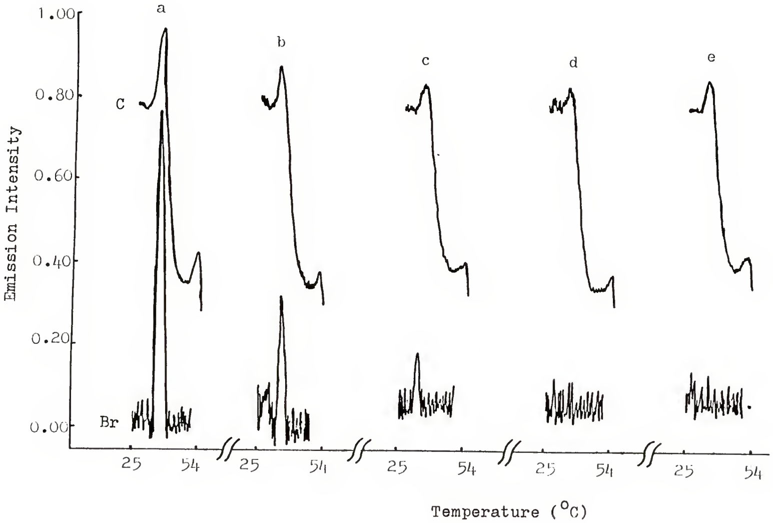
a
b
c
d
e
C
Br
1.00
0.80
0.60
0.40
0.20
0.00
Emission Intensity
25
54
Temperature (°C)

Figure 17. Decay of $C_2H_4Br_2$ by stirring of solution. Experimental conditions: microwave power = 500 W; Br emission wavelength = 827.2 nm.

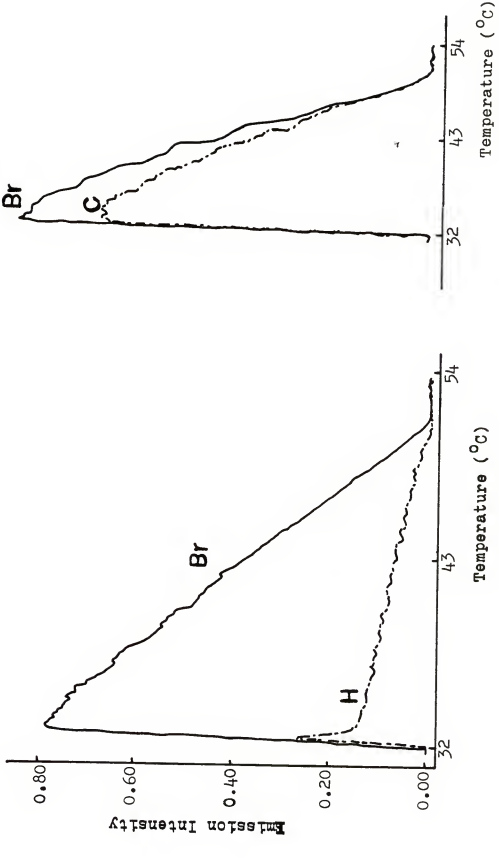
Emission Intensity
0.80
0.60
0.40
0.20
0.00
32
43
54
Temperature (°C)
Br
H
Br
C
32
43
54
Temperature (°C)

crucible temperature reached 32°C and dropped back to baseline before the sample crucible temperature reached 54°C. Signals with one or two peaks could be observed. The presence of either one or two peaks might be due to the He carrier gas flow rate, which might not have been at its optimum value. Similar phenomena occurred in Chapter IV, where the low He carrier gas flow rate also resulted in two peaks.

Speciation of $C_2H_4Br_2$

Figure 18 shows the simultaneous chart recording of H and Br and of C and Br. The final concentrated solution (25 mL) was used in these measurements. Since the emission signals of C, H, and Br appeared at the same time, the $C_2H_4Br_2$ may have been vaporized as a molecular species; therefore the sample of $C_2H_4Br_2$ most likely was freeze preconcentrated with no change in chemical form.

Figure 18. Single electrode microwave emission of Br, C and H in $C_2H_4Br_2$ by thermal gas evolution. Experimental condition: microwave power = 500 W; emission wavelengths: Br = 827.2 nm; H = 656.2 nm; C = 247.8 nm.

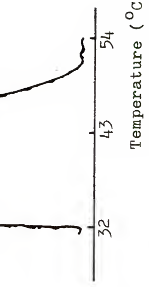
Br
C
32
43
54
Temperature (°C)

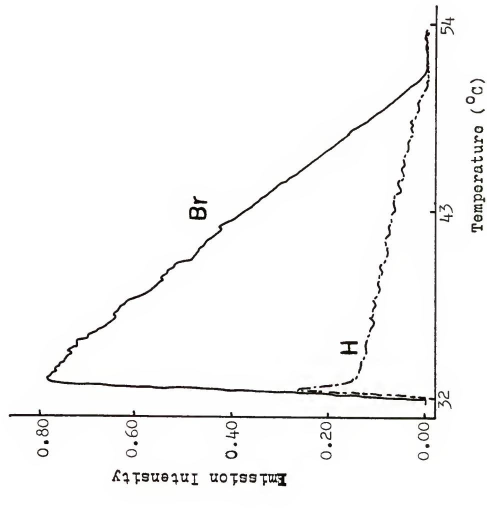
Emission Intensity
0.80
0.60
0.40
0.20
0.00
Br
H
32
43
54
Temperature (°C)

CHAPTER III
DEVELOPMENT OF LONG ABSORPTION CELL FOR ATOMIC ABSORPTION SPECTROSCOPY

Background Introduction

Graphite Furnace Atomic Absorption Spectrometry

In 1955, the first two papers were published describing atomic absorption as an analytical technique. Alkemade and Milatz (33), from the Netherlands, used a flame as a source and a second flame as an absorption cell. In Australia, Walsh (34) described an instrument with an AC detection system and hollow cathode lamp as a sharp line source of radiation for the element of interest. In 1961, L'vov (35) described an electrically heated graphite furnace providing an atomic absorption environment to detect picogram quantities of analyte. In 1966, Massmann (36) developed a simpler furnace based upon the experience of L'vov. In 1968, Woodriff (37) designed a more complicated and much longer graphite furnace to increase the absorption signal. These three kinds of tube furnaces and the Varian type furnace, that have received extensive experimental study, are shown in Figure 19. Comparisons of these four furnaces are given in Table 11. In the Massmann furnace, sample is added to the cold tube

Figure 19. Electrothermal atomizer chambers used in atomic absorption spectrometry.

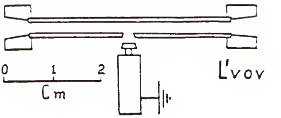
Cm
L'vov

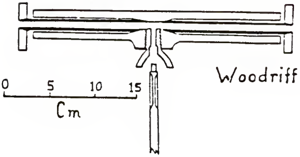
Cm
Woodriff

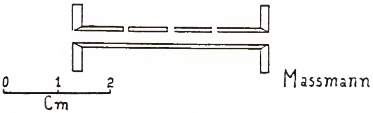
Cm
Massmann

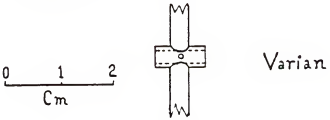
Cm
Varian

Table 11. Comparisons of Dimensions of Electrothermal Tube Furnaces.

	Representative interior atomizer dimensions (mm)	
	Length	Diameter
L'vov	40	2.5
Woodriff	300	7
Massman	55	8
Varian	9	3

with a pipet through the center hole. The tube is heated in three steps to dry, ash, and atomize the sample. This furnace is a semi-enclosed system. The operation is easy, but sample can be lost from the center hole. This is especially critical for very volatile samples when the atomization time is longer than the vaporization step. L'vov found that when a transverse hole of 2- or 3-mm diameter was used for sample introduction, 20% to 40% of the sample diffused through it.

The L'vov and Woodriff furnaces both operate isothermally; in both, sample is inserted into the preheated furnace for drying, ashing, and atomization. However, in the L'vov furnace, sample is dried and ashed by an auxiliary power supply without cooling the furnace, and it is heated to reach the atomization temperature. In the Woodriff furnace, sample is dried and ashed before insertion into a much longer graphite furnace and then atomized.

The Varian furnace is also called a mini-Massmann furnace. An advantage of this design is that the tube can be heated rapidly and uniformly, because the tube is very short. Figure 20 shows the variation in the surface temperature of the furnace with the distance from the center (38). Another advantage results from the high atom densities created by its smaller cross-sectional area. The disadvantage is that sample will quickly escape from both ends of the tube, because the residence time becomes

Figure 20. Variation with time of the Varian furnace surface temperature along the length of the graphite tube at a furnace heating rate of 1.10 K ms^{-1}. The time shown below represents the time elapsed after the commencement of the atomization cycle. (A) 0.45 s, (B) 0.65 s, (C) 0.85 s, (D) 1.05 s, (E) 1.25 s. Adapted from (38).

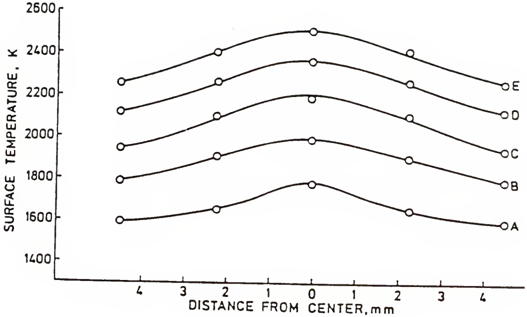
SURFACE TEMPERATURE, K
2600
2400
2200
2000
1800
1600
1400
E
D
C
B
A
4
3
2
1
0
1
2
3
4
DISTANCE FROM CENTER, mm

shorter. The resident time of atoms in the tube is proportional to the square of the tube length. When real samples are analyzed, as the matrix material becomes gaseous, it tends to sweep the analyte atoms out of the chamber, unless the chamber is very long. Woodriff (39) showed that the overall relative sensitivity is proportional to the tube length cube.

The relationship of furnace length, temperature, and pressure to peak height and peak area will be given in the section of theoretical considerations.

The pulse-heated atomizer, such as the Massmann furnace, which is the one most widely used in graphite furnace atomic absorption spectrometry (GFAAS), has been found to be very prone to serious matrix interferences (40). Remedies such as preliminary separation of analyte from interferents and standard addition calibration are time-consuming and the latter may not eliminate bias that arises from matrix effects. The addition of modifiers as well as pretreatment of the graphite surface and alteration of the analyte-matrix chemistry (41) are means of reduction of matrix interferences. Matrix modifiers shift the appearance temperature of the analyte, which reflects the change of activation energy of the atomization process, and minimize the loss of atoms due to molecular vaporization. However, the actual reaction mechanisms of matrix modifiers are still generally unknown (42,43).

Many expressions have been derived to describe the relationship between atomizer heating rate and peak height absorbance for electrothermal atomization under nonisothermal and isothermal conditions. The results of deGalan et al. (44), which are given in Table 12, indicate peak height and peak area absorbances for 0.5 ng of Pb in aqueous solution and in the presence of 1 μg of $NaNO_3$, respectively, under isothermal and nonisothermal conditions. The matrix in this case, $NaNO_3$, influenced the rate of atom formation under nonisothermal conditions. In addition, fast atomization under isothermal condition brings the recovery close to 100%.

Chang and Chakrarbati (45) found that higher heating rates enhanced the maximum atom population inside the furnace and resulted in shifting the atom peak profile, i.e., population vs time, towards the constant temperature region. Moreover, long tubes as well as high heating rates, which maximize the ratio of atom formation rate constant k_1, in s^{-1} ($k_1 = A \exp[-E_a/RT]$; E_a, A, R, and T are the activation energy of the rate-determining step, frequency factor, gas constant, and absolute temperature) to atom loss rate constant k_2 in s^{-1} ($k_2 = 8D/L^2$; D and L are the diffusion coefficient of the diffusing gas and the length of graphite tube), result in the highest peak height absorbance. Figures 21 and 22 show the effect of the heating rate and the tube length on the maximum atom

Table 12. Peak Height and Peak Area Absorbance for 0.5 ng of Lead in Aqueous Solution and in the Presence of 1 µg of Sodium Nitrate, Respectively. Atomization Was Performed at Constant Tube Temperatures.

Isothermal tube temperature (°C)	Pb in H_2O		Pb in $NaNO_3$		Recovery rel. H_2O (%)	
	Peak height (A)	Peak area (As)	Peak height (A)	Peak area (As)	Peak height	Peak area
1510	0.25	0.156	0.29	0.155	116	100
1680	0.36	0.152	0.34	0.153	94	101
1920	0.41	0.148	0.38	0.146	94	99
2180	0.45	0.136	0.43	0.126	95	93
Non-isothermal atomization[a]	0.26	-	0.20	-	78	-

[a] The final tube temperature was 1800°C.

Adapted from (44).

Figure 21. Effect of the heating rate on the maximum atom population, N_{max}, with activation energy as a parameter. General parameters: T_c = 700 k, T_f = 2500 k, A = $1.0x10^{12}$ s^{-1}, L = 2.0 cm, D_o = 0.10 cm^2s^{-1}, n = 1.8; E_a = (kJ mol^{-1}): 400, 450, 480, 500, 530. Adapted from (45).

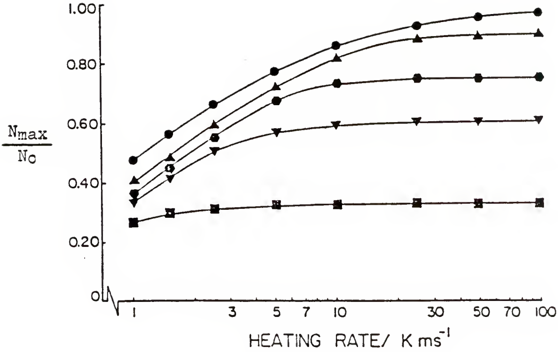
1.00
0.80
0.60
0.40
0.20
0
$\frac{N_{max}}{N_o}$
1
3
5
7
10
30
50
70
100
HEATING RATE/ K ms^{-1}

Figure 22. Effect of the tube length on the maximum atom population, N_{max}, with activation energy as a parameter. General parameters: $A' = 1.0 \times 10^{12}$ s^{-1}, $T_c = 700$ k, $T_f = 2500$ k, $\alpha = 5.0$ k ms^{-1}, $D_o = 0.10$ cm^2 s^{-1}, $n = 1.8$; activation energy (kJ mol^{-1}): 400, 450, 480, 500, 530. Adapted from (45).

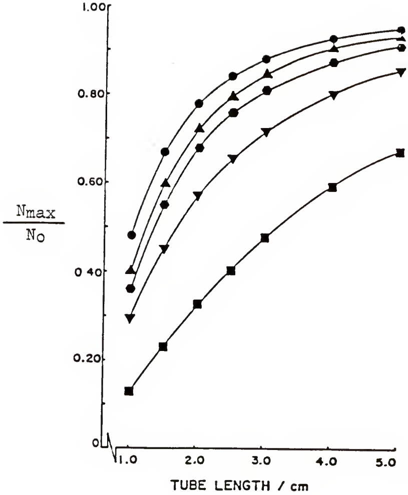
1.00
0.80
0.60
0.40
0.20
0
Nmax
No
1.0
2.0
3.0
4.0
5.0
TUBE LENGTH / cm

population, N_{max} (number of atoms), with activation energy as a parameter. What can be concluded is that current attempts to attain more nearly isothermal conditions in a pulse-heated furnace have strong justification, from both theoretical and experimental research.

Since the sample vaporization step can cause interferences (molecular absorption, light scattering, and atom and molecule loss) on the analyte absorption signal, independent control of vaporization and atomization should result in higher sensitivity, greater freedom from interferences, and more efficient atomization of analytes (46). The use of electrothermal techniques for atomic absorption spectrometry and for introduction of samples into plasmas is gaining popularity (47). The latter use reduce the sample volume required for analysis, compared to the conventional nebulization system, and permit more efficient introduction of the sample directly into the plasma region by minimizing the solvent background and interference effects. In Table 13, a comparison is given of detection limits for ICP (inductively coupled plasma) with electrothermal vaporization and pneumatic nebulization, and GFAAS by Long et al. (48).

It is the aim of this work to evaluate an improved long graphite atomization cell, which was designed based upon three criteria in GFAAS, namely use of a long

Table 13. Comparison of Detection Limits for Electrothermal Vaporization and Pneumatic Nebulization from Previous Studies.

		ICP			
Element	λ/nm	Graphite rod (10 μl)	Carbon cup (10 μl)	Neb[a] (continuous)	Graphite furnace AAS (5 μl)
Ag	328.1(I)	0.1	0.3	4	0.04
Al	396.2(I)	2	2	-	6
As	228.8(I)	200	20	40	20
Au	242.8(I)	-	1	40	2
	267.6(I)	1	-	-	-
Be	234.9(I)	0.1	-	0.5	-
Bi	289.8(I)	-	10	-	1.4
Ca	422.7(I)	0.002	-	0.07	-
Cd	228.8(I)	3	1	2	0.02
Co	238.9(I)	-	3	-	1.2
Cu	324.8(I)	0.2	1	11.4	
Fe	259.9(II)	2	-	5	0.6
	372.0(I)	-	3	-	-
Ga	417.2(I)	1	-	14	-
Ge	303.9(I)	-	1	-	-
Hg	253.7(I)	6	1	200	20
K	404.7(I)	-	300	-	0.18
In	325.6(I)	2	-	30	-
Li	670.8(I)	0.4	0.6	-	1
Mg	279.6(II)	0.01	-	0.7	0.01
	285.2(I)	-	0.01	-	-
Mn	257.6(II)	0.1	-	7	0.1
	279.5(I)	-	0.1	-	-
Ni	352.4(I)	-	4	-	2
P	213.6(I)	20	-	40	-
Pb	405.8(I)	10	10	8	1
Re	346.0(I)	10	-	-	-
Rb	420.2(I)	-	280	-	1.2
Sn	327.5(I)	-	5	200	12
Sb	259.8(I)	30	-	200	-
Tl	377.6(I)	-	5	200	0.6
	535.0(I)	6	-		
Zn	213.8(I)	0.2	0.3	2	0.02

All detection limits ng ml^{-1}.

Adapted from (48).

[a] Nebulization.

and isothermal furnace with independent sample introduction system.

Arsenic and antimony were selected as analytes. A hydride generation system was chosen to produce arsine and stibine before introduction into the atomization cell. Because arsine and stibine are gases at room temperature, less problems occur during the transport process. In addition, arsine and stibine do not need very high atomization temperature (900°C-1200°C) to be atomized. The variations of furnace temperature, the Zeeman effect, the effect of an inner tube, and analytical figures of merit will be described.

Hydride Generation

In the 1960s and early 1970s, there were difficulties associated with the determination of elements such as antimony, arsenic, selenium, tellurium, etc. by conventional flame AAS. Optimal analytical absorption lines of these elements lie in the far ultraviolet region of the spectrum (below 230 nm), where the background absorption due to the commonly used flames is large, causing unfavorable signal-to-noise ratios (49). In addition, other problems arise with GFAAS; at the short wavelengths of interest, scattering by particulate matter, such as carbon, is severe and matrix interferences are unavoidable. Furthermore, analyte loss can occur during the charring or ashing stage especially for these relatively volatile elements (antimony, arsenic, selenium, tellurium, etc.).

In 1969, Holak (50) utilized the well-known arsine generation procedure (the classical Marsh reaction and the Gutzeit method) for the determination of arsenic. Arsine was generated by reaction of Zn with HCl and collected in a liquid N_2 trap. Nakahara (51) has summarized in detail the principal advantages and disadvantages of utilizing the hydride generation techniques for atomic spectrometric analysis.

Several reducing agents and sources of nascent hydrogen have been investigated for use in reduction of the element of interest to its covalent hydride for analytical purposes. Presently, there are two main reactions for hydride generation. The earlier technique is generally classified as a metal-acid system such as Zn-HCl reduction. The major drawback of this reaction is that it can be only used for As, Sb, and Se, and the time taken for the completion of the reaction may be as long as 10 min. The newer and more effective method for the production of the hydrides involves the use of $NaBH_4$-acid reaction. Reaction is shown in the following equation:

$$NaBH_4 + 3H_2O + HCl \rightarrow H_3BO_3 + NaCl + 8H^{\bullet}$$

$$(n+m)H^{\bullet} + E^{n+} \rightarrow EH_n + \frac{m}{2} H_2$$

where E is the analyte of interest. $NaBH_4$ was used for atomic spectrometric application in 1973 by Schmidt and Royer (52). The $NaBH_4$-acid reduction was found to be superior to the metal-acid reduction system with respect to reduction yield, short reaction time, minimal contamination of the blank, and applicability to the element concerned. Collection times were reduced to 30 s for Bi and Te, and 2-3 min for As, Ge, Sb, Se, and Sn (53).

The hydride evolved either is conveyed directly into the atomization system ("direct-transfer mode") or some form of storage is used before transferring to the atomizer ("collection mode"). Collection procedures have been proposed for the hydrides which are slowly evolved, such as AsH_3, whereas SbH_3, which is formed very rapidly and is unstable in the gas phase, should be transferred directly to the atomizer (54).

Therefore, As and Sb were selected as analytes in our experiments. In addition, it is interesting to compare the two introduction methods: direct-transfer mode and collection mode. Concentrations of reagents and HCl were chosen from related papers, in which optimum reagent concentrations and acid concentration were carefully studied. Different characteristics of AsH_3 and SbH_3 will be discussed. Carrier gas flow rate effect, liquid N_2 trapping time effect, and the interelement interference effect will be described. Some NBS standard reference materials will be analyzed and compared.

Theoretical Considerations

On the basis of the ideas formulated by Mandel'shtam (55) and later by Raikbaum (56), L'vov (57) further derived equations to represent sample atomization taking place within a cell through which sample passes. The cell is taken as the volume which directly participates in producing the analytical signal observed by the experimenter. For the sake of simplicity and general discussion, the drying and ashing stages are eliminated; any complicating processes that might accompany the transport of substance through the cell, such as dissociation of molecules and ionization of atoms are ignored, and all elements are assumed in the atomic state while inside the cell. The following symbols will be used:

N_o: number of atoms of an element in the sample.

N: number of atoms entering the analysis volume at any instant of time.

t_1: the overall length of time during which atomization occurs (the atomization time).

t_2: the mean length of time spent by an atom in the analysis volume (the residence time).

$n_1(t)$: number of atoms entering the analysis volume in unit time.

$n_2(t)$: number of atoms escaping from the analysis volume in unit time.

The balance between the number of atoms entering the analysis volume, $n_1(t)$, and escaping from it, $n_2(t)$, in unit time is given by

$$\frac{dN}{dt} = n_1(t) - n_2(t) \qquad (10)$$

The form of functions $n_1(t)$ and $n_2(t)$ depends on the method of atomization used. We can approximate the function as

$$n_1(t) = \frac{N_o}{t_1} \qquad (11)$$

$$n_2(t) = \frac{N}{t_2} \qquad (12)$$

Equations 11 and 12 are valid for a uniform process of transfer of atomic vapor to the analysis volume and for the loss of atoms by diffusion. Equation 10 can be rewritten in the form

$$\frac{dN}{dt} = \frac{N_o}{t_1} - \frac{N}{t_2} \qquad (13)$$

By resolving the variables and integrating Equation 13, the following equation for the instantaneous values of N at times, when t is both less than and greater than t_1, are given by

$$N_{t\leq t_1} = N_o \frac{t_2}{t_1}(1 - e^{-t/t_2}) \tag{14}$$

$$N_{t>t_1} = N_o \frac{t_2}{t_1}(1 - e^{-t/t_2})\ e^{-(t-t_1)/t_2} \tag{15}$$

Figure 23 shows the variation in the number of atoms for different ratio t_1/t_2. As the value of t increases (high t_1/t_2 ratio), the magnitude of N tends to distribute more dispersedly. At the moment when a sample has been totally atomized ($t=t_1$), N reaches its peak value:

$$N_{peak} = N_o \frac{t_2}{t_1} (1 - e^{-t_1/t_2})$$

If $$t_1/t_2 << 1,\ 1 - e^{-t_1/t_2} \approx \frac{t_1}{t_2} \tag{16}$$

and so $$N_{peak} = N_o \tag{17}$$

If a sample is completely atomized, in a length of time much shorter than the time spent by the atoms in the cell (see Equation 17), the peak value N_{peak} must correspond to the total number of atoms in the sample. It is quite remarkable that the variations in the values of t_1 and t_2 which may take place during measurements have practically

Figure 23. Variation in the number of atoms in an analysis volume for different ratios t_1/t_2. 1, $t_1/t_2 = 0.2$; 2, $t_1/t_2 = 1$; 3, $t_1/t_2 = 5$. Adapted from (57).

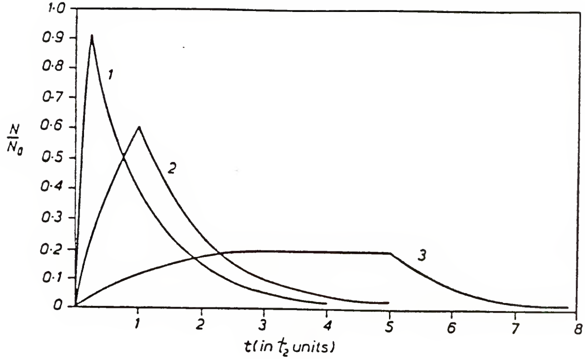
1·0
0·9
0·8
0·7
0·6
0·5
0·4
0·3
0·2
0·1
0
$\frac{N}{N_0}$
1
2
3
0
1
2
3
4
5
6
7
8
t(in t_2 units)

no effect on N_{peak}/N_o, provided that the condition $t_1/t_2 << 1$ is fulfilled. Figure 24 shows the typical representation of t_1, t_2, and the furnace atomizer absorbance signal (58).

In fact, trends to produce the next generation of GFAAS are more or less following the above considerations. For instance, a higher heating rate and an isothermal graphite furnace have been proposed to decrease the atomization time, t_1 (45). Matrix modifiers, the L'vov platform, and a longer graphite tube increase the atom residence time, t_2 (59).

The relationship of furnace length, temperature, and pressure to peak height and peak area was also evaluated by L'vov (57) for the constant-temperature furnace. Diffusion-controlled atom loss and the condition $t_2 >> t_1$ are required to fulfill the above limiting conditions. The absorbance peak height and peak area can be expressed as:

$$A_{peak} \propto (f/A_w S \Delta\nu_s)\ M \tag{18}$$

$$A_{area} \propto (f t_2/A_w S \Delta\nu_s)\ M \tag{19}$$

where f is the oscillator strength of the atomic absorption line, A_w is the atomic weight of the element concerned and M its mass in grams, S is the transverse cross-sectional area of the furnace, and $\Delta\nu_s$ is the displacement of the frequency maximum of a line relative to its initial

Figure 24. Furnace atomizer absorbance-time profile. Legend: A = atomization, B = peak height, C = diffusion, D = end of the power cycle, t_1 = atomization time, t_2 = residence time. Adapted from (58).

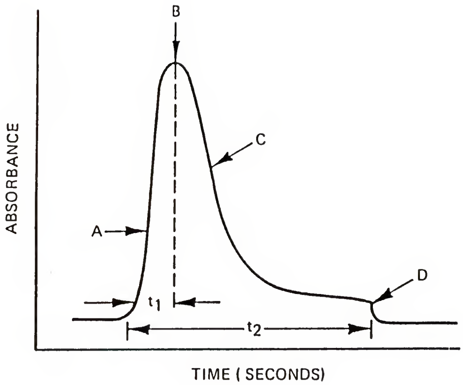
B
C
A
D
t_1
t_2
ABSORBANCE
TIME (SECONDS)

position as a result of a change in pressure of a foreign gas and/or temperature. For a furnace operated at atmospheric, the Lorentz contribution to $\Delta\nu_s$ is usually small. The measured absorbance terms can also be expressed as

$$A_{peak} \propto (T^{0.7}/S)\ M \tag{20}$$

$$A_{area} \propto (L^2/ST^{0.9})\ M \tag{21}$$

From those equations above, both measuring methods are inversely proportional to the cross-sectional area of the furnace. Thus, small diameter furnaces are preferable where physically possible (factors such as light throughout and blackbody emission must be considered). When integrated absorption is measured, the length of the cuvette becomes of great importance. The cuvette length also will be limited by the power input and the luminous flux passing through the cuvette from the source.

Examples for the use of the above equations will be given in the section on results and discussion.

Experimental Section

Apparatus

Long graphite absorption cell AAS. A Hitachi Model 180-80 atomic absorption spectrometer equipped with a laboratory-constructed 14 cm long graphite tube furnace, hallow cathode lamp (Hamamatsu), and a Hitachi Model 056 strip-chart recorder were used. The cross-sectional view of the long absorption cell is shown in Figure 25. The cell consists of a central graphite tube as the resistive heating element. An inner tube was placed inside the central tube. Two graphite electrodes hold the heater tube ends, allowing for expansion as well as providing good electrical contact, and two brass electrodes with inside cooling water tubes hold the graphite electrodes. A sample gas inlet tube, which was held by a threaded graphite tube holder, was inserted into the inner tube. The entire absorption cell was housed inside a quartz cylinder. Helium gas carried the sample gas into the sample inlet tube, and argon carrier gas was introduced to the carrier gas inlet tube. Argon or nitrogen gas, as sheath gas, and power supply cables were connected through terminals to the brass electrodes. Table 14 shows the instrument settings.

Hydride generation system. Figure 26 shows the block diagram of the hydride generation system coupled with the long absorption cell; F is the hydride collector which includes a 9 mm O.D. Pyrex U-tube (30 cm length) filled with glass beads and immersed in liquid N_2 solution. The apparatus used for the generation of arsine was similar to the one described by Uthus, Collings, Cornatzer, and Nielsen (60). Helium (b.p. -252.77°C) was used as the

Figure 25. Cross-sectional view of long absorption cell.

Legend:
1. inner tube: I.D. 4.5 mm, O.D. 6.5 mm, length 19 cm, alumina;
2. quartz tube: O.D. 25 mm, length 14 cm;
3. tube heater: I.D. 6.5 mm, O.D. 9.5 mm, length 14.5 cm, graphite;
4. sample gas inlet tube: alumina;
5. carrier gas inlet tube: alumina;
6. sample gas inlet tube holder: graphite;
7,8. graphite electrode;
9,10. terminal;
11. quartz window;
12. insulator;
13. electrode cooling water tube;
14. sheath gas inlet;
15. electrode assembly holder: brass;
16. electrode assembly holder binding bar: brass.

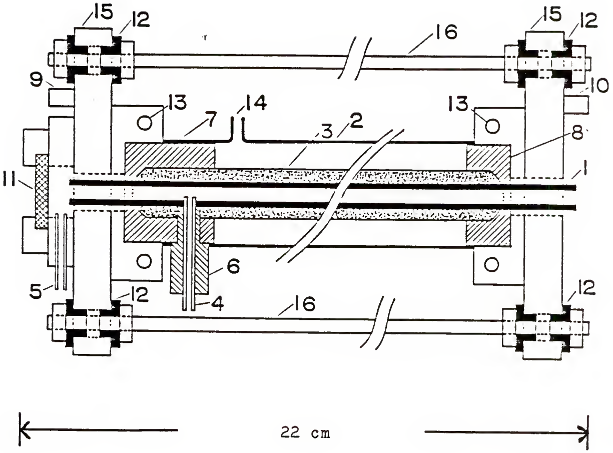
22 cm

Table 14. Instrument Settings of Long Absorption Cell Hitachi Atomic Absorption Spectrometer System.

light source	hollow cathode lamp
cuvette	14 cm graphite tube
power supply	SCR power supply Model SCR 20-250, Electronic Measurements Inc., Neptune, N.Y.
sheath gas	argon
slit width	As (2.6 nm), Sb (0.4 nm)
wavelength	As (193.7 nm), Sb (217.5 nm)
recorder	10 mV (full scale)

Figure 26. Block diagram (not to scale) of arsine and stibine generation system. Legend: (A) helium, (B) generating flask, (C & D) cold traps to collect water, (E) $CaCl_2$ drying tube, (F) liquid N_2 cold trap, (G) argon.

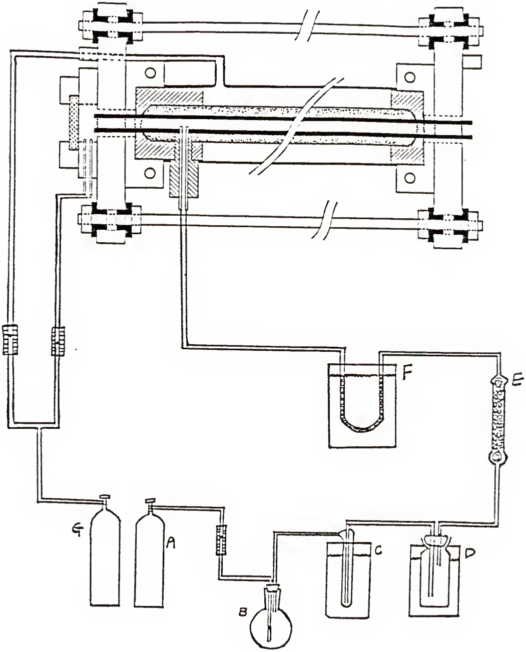
F
E
G
A
C
D
B

arsine carrier because it has a lower boiling point than liquid N_2 (b.p. -195.79°C), which avoids clogging that would take place with argon (b.p. -185.86°C). The argon line from the gas cylinder was split, by using a glass y-joint, into two lines provided with separate flow-meters. One line was connected to the left side inlet of the graphite tube to sweep the helium/arsine mixture into the furnace; the other line was connected to the quartz tube as a sheath gas to minimize degradation of the graphite heater tube.

GFAAS. The same process was used as described in Chapter II.

Flame AAS. A Hitachi Model 180-80 atomic absorption spectrometer equipped with a 10 cm slot burner for air/acetylene, hollow cathode lamp (Hamamatsu), and a Hitachi Model 056 strip-chart recorder were used. Sample was introduced as the hydride produced through the hydride generation system. Table 15 shows the instrument settings.

SEMPES. The same process was used as described in Chapter II.

Reagents

All the graphite parts are POCO graphite grade HPD-3 (61). Standard stock solutions of arsenic and antimony were prepared by dissolving As_2O_3 (SRM 83b, NBS) and $K(SbO)C_4H_4O_6 \cdot 1/2H_2O$ (A.C.S. grade, Fisher Scientific). The

Table 15. Instrument Settings for Hitachi Flame Atomic Absorption Spectrometry.

light source	hollow cathode lamp
burner height	7.5
oxidant/fuel	air (9.4 L/min)/C_2H_2 (2.3 L/min)
wavelength	As (193.7 nm), Sb (217.5 nm)
slit width	As (2.6 nm), Sb (0.4 nm)
recorder	10 mV (full scale)

10% (w/v) aqueous $NaBH_4$ solution was prepared daily by dissolving $NaBH_4$ (A.C.S. grade, Fisher Scientific) in 0.5% (w/v) aqueous KOH (86%, Mallinckrodt); the KOH stabilized the $NaBH_4$ (51). The $NaBH_4$ solution was left aside for at least 30 min, and the upper clean solution was used. The 20% (w/v) KI was prepared by dissolving KI (A.C.S. grade, Fisher Scientific) in deionized water.

Procedures

Preparation of NBS standard reference materials (SRM). The NBS SRMs were dried in a desiccator for two days using P_2O_5 as the drying agent. Approximately 250 mg of samples (orchard leaves, SRM 1571; tomato leaves, SRM 1573; bovine liver, SRM 1577a) were weighed into a 300-mL round bottom flask, and then 20 mL high purity HNO_3 and 1 mL of the H_2SO_4 solution (18 M) were added. The sample/acid mixture was digested with a condenser and a laboratory-constructed HNO_3 acid reservoir. A side arm reservoir was used to collect the condensed HNO_3 after the H_2SO_4 produced white fumes; the flask was then cooled down and the condensed HNO_3 solution was returned to the sample mixture. The digestion procedure was repeated until the H_2SO_4 residual solution became clear. The solution was transferred into a Teflon beaker and evaporated until H_2SO_4 produced white fumes. Finally, the digested solution was transferred into a 50 mL volumetric flask and diluted with deionized water to the mark. This sample was then used directly for arsenic or antimony measurements. Standard calibration solutions were prepared in 100-mL flasks from 1000 ppm stock solutions of arsenic and antimony with a suitable amount of HCl (4%).

Hydride generation. For arsine generation, the 1-mL sample was placed in the 100-mL round bottom flask with 1 mL of 20% KI, 2 mL of deionized water (1 mL for stibine generation), and 1 mL of 6 M high purity HCl (2 mL for stibine). The solution was stirred, 1 mL of the $NaBH_4$ solution was added, and the arsine or stibine was collected in the liquid N_2 trap. This process required about 6 min. The optimum concentrations of HCl, KI, and $NaBH_4$ were selected from previous studies (62-64). It was required to purge the helium gas for 2-3 min to remove oxygen from the system before immersing the U-tube into liquid N_2 solution; otherwise, the pressure change resulting from the boiling of oxygen in the U-tube would disturb the hydride transport. The graphite furnace was turned on and kept at a constant temperature before transferring the liquid N_2 dewar flask to a beaker, which was filled with room temperature water. The recorder was turned on to record the arsenic and antimony atomic absorption signals.

Results and Discussion

Determination of Arsenic and Antimony

The measurement of As and Sb was first tested by the two sample introduction methods: the direct transfer mode and the collection mode. Figures 27 and 28 show the absorption signal difference between these two methods for As and Sb, respectively. The hydride collection time in the collection mode is 6 min for As and Sb, as used by Shaikh and Tallman (65). In the latter paper, the arsine was trapped in a small volume of a chloroform/ephedrine solution containing silver diethyldithiocarbamate (SDDC). The relationship between the relative absorbance and the trapping time will be discussed in detail in the section on liquid nitrogen trapping time.

Figure 29 shows the temporal profiles (absorbance vs time) by Chapman and Dale (66). The plots were obtained sequentially by the direct transfer mode for 500 ng of Sb, As, Pb, Se, Te, and Sn, and 100 ng of Bi. They suggested a collection procedure should give higher sensitivity for As and Sb, because their hydrides showed slower evolution, which agreed well with our results in Figures 27 and 28.

The Sb sensitivity using direct transfer is larger than As, but both As and Sb have poor reproducibility (see Figures 27 and 28). The temporal peak depends on kinetic factors of hydride evolution, such as injection speed of

Figure 27. Comparison of sample introduction methods for 10 ng As. Experimental conditions: a, direct transfer; b, collection time 6 min; absorption wavelength = 193.7 nm.

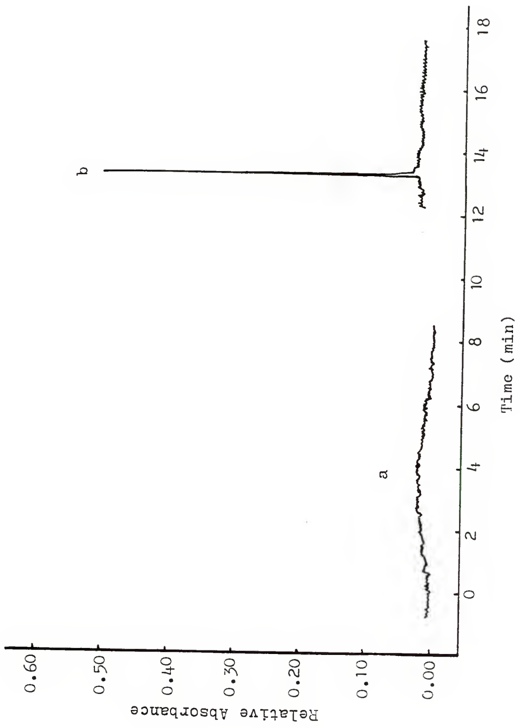
Relative Absorbance
0.60
0.50
0.40
0.30
0.20
0.10
0.00
Time (min)
0
2
4
6
8
10
12
14
16
18
a
b

Figure 28. Comparison of sample introduction methods for 10 ng Sb. Experimental conditions: a, direct transfer; b, collection time 6 min; absorption wavelength = 217.5 nm.

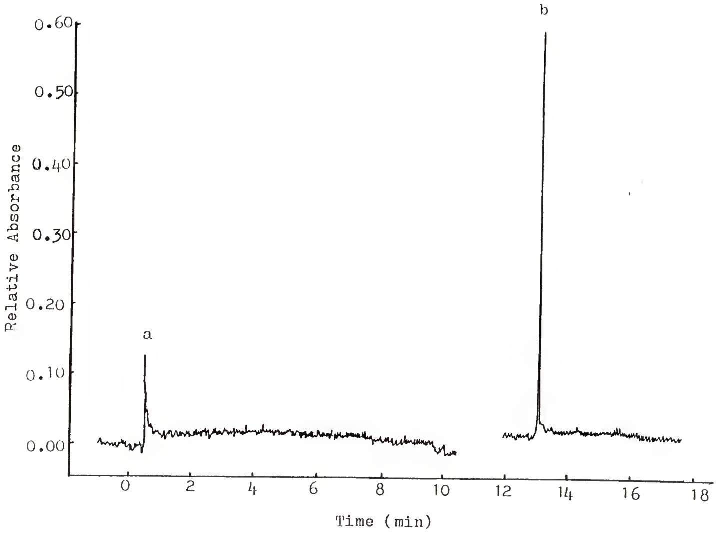
a
b
Relative Absorbance
0.00
0.10
0.20
0.30
0.40
0.50
0.60
Time (min)
0
2
4
6
8
10
12
14
16
18

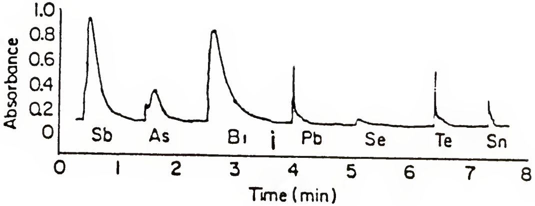

Figure 29. Absorbance vs time plots obtained by the direct transfer mode for 500 ng of each element except bismuth (100 ng). Adapted from (66).

$NaBH_4$ solution into the reaction flask, stirring rate of the reaction solution, the carrier gas flow rate, and the transport efficiency. In addition, tailing in the direct transfer mode lasts for about 10 min, whereas in the collection mode (6 min), most of the hydride was trapped and carried out in a plug by carrier gas, but a trace of absorbance signal still could be observed for 4 min after the liquid N_2 trap was removed. Collection mode was used in our experiments, because more reproducible signals were obtained. Although the antimony signal in the direct transfer mode appears first and is of higher sensitivity, the completion of stibine evolution has a longer tail than that of arsine.

Precision and Accuracy

By using the long absorption cell, the limits of detection are 0.2 ng/mL and 0.1 ng/mL (S/N=3) with RSD of 2-3% for As and Sb, respectively; Table 16 shows the comparison of detection limits (ng/mL) for analytical atomic spectrometric methods utilizing hydride generation (51). Arsenic and Sb contents of various NBS standards were analyzed. As shown in Table 17, the values obtained for the six determinations agreed well with the NBS values. Concentration of Sb in tomato leaves (1573) was not reported in NBS value, so it was also not measured in our laboratory. All data shown have proved this technique to be of high precision and accuracy.

Table 16. Comparison of Detection Limits (ng/mL) for Analytical Atomic Spectrometric Methods Utilizing Hydride Generation (S/N = 3).

Element	AAS[a]	AES[b]	AFS[c]	Present Study
As	1.2	0.3	0.2	0.2
Sb	0.8	1.5	0.2	0.1

AAS: Atomic Absorption Spectrometry; AES: Atomic Emission Spectrometry; AFS: Atomic Fluorescence Spectrometry.

[a] Ref. 67

[b] Ref. 68

[c] Ref. 69.

Table 17. Arsenic and Antimony Content of NBS Standard Reference Materials Measured by Collection Hydride Generation and Long Absorption Cell Atomic Absorption Spectrometry.

SRM	Element	No. of samples	Present study (µg/g dry weight)	NBS Certified Value (µg/g dry weight)
1571 orchard leaves	As	6	10 ± 1	10 ± 2
	Sb	6	2.9 ± 0.2	2.9 ± 0.3
1573 tomato leaves	As	6	0.28 ± 0.03	0.27 ± 0.05
1577a bovine liver	As	6	0.046 ± 0.005	0.055 ± 0.006
	Sb	6	0.005 ± 0.002	(0.005)[a]

[a] Uncertified value.

Effect of Carrier Gas Flow Rate

The effect of argon (or helium) carrier gas flow rates on peak height absorbances of As and Sb are shown in Figures 30 and 31, respectively. An argon carrier gas flow rate of 120 mL/min gives maximum absorption for samples containing 10 ng/mL of As or Sb, and helium carrier gas flow rates of 55 mL/min and 100 mL/min give maximum absorption for the same concentration samples of As and Sb, respectively.

Low carrier gas flow rate would decrease the absorption signal and sometimes cause the peak to split into two peaks, while high flow rate probably resulted in incomplete dissociation, because of the shorter residence time in the absorption cell. The split peaks at the low flow rate explain the nonreproducible $C_2H_4Br_2$ peaks in Figure 14 in Chapter II. Optimum helium flow rate for the determination of Sb agreed with the paper by Andreal et al. (70). Stronger adsorption of stibine to the glass beads might explain why a higher helium flow rate (see Figure 31) is needed to carry out the stibine.

Liquid Nitrogen Trapping Time

Figure 32 shows that the arsine signal reached a plateau in about 6 min. This result agrees with the experiment by Shaikh and Tallman (65).

The effect of the first 6-min trapping time for Sb is the same as in As; nevertheless, the relative absorbance

Figure 30. Effect of helium flow rate on peak height absorption signal for collection mode-hydride generation-long absorption cell atomic absorption spectrometry. Legend: Δ, 5 ng As; o, 5 ng Sb. Experimental condition: absorption wavelengths, As = 193.7 nm and Sb = 217.5 nm.

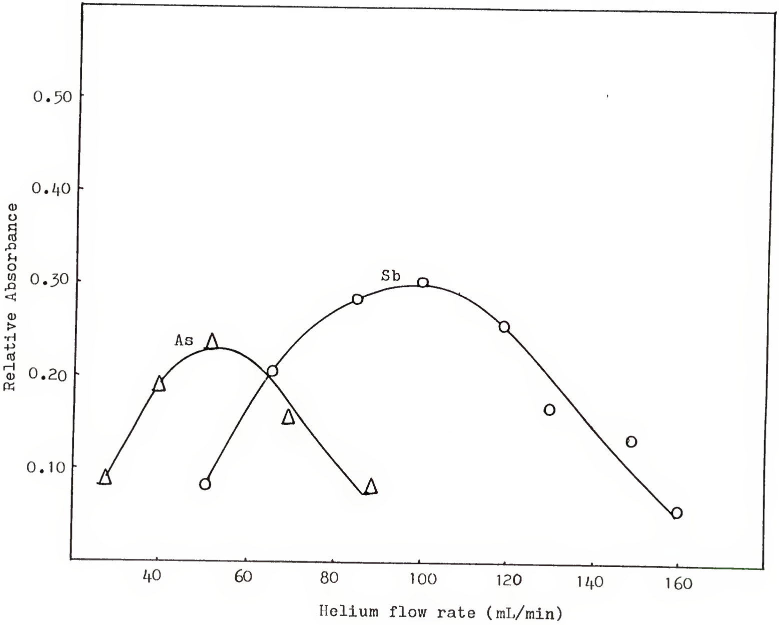

0.50
0.40
0.30
0.20
0.10
Relative Absorbance
As
Sb
40
60
80
100
120
140
160
Helium flow rate (mL/min)

Figure 31. Effect of argon flow rate on peak height absorption signal for collection mode-hydride generation-long absorption cell atomic absorption spectrometry. Legend: Δ, 10 ng As; ○, 10 ng Sb. Experimental condition: absorption wavelengths, As = 193.7 nm and Sb = 217.5 nm.

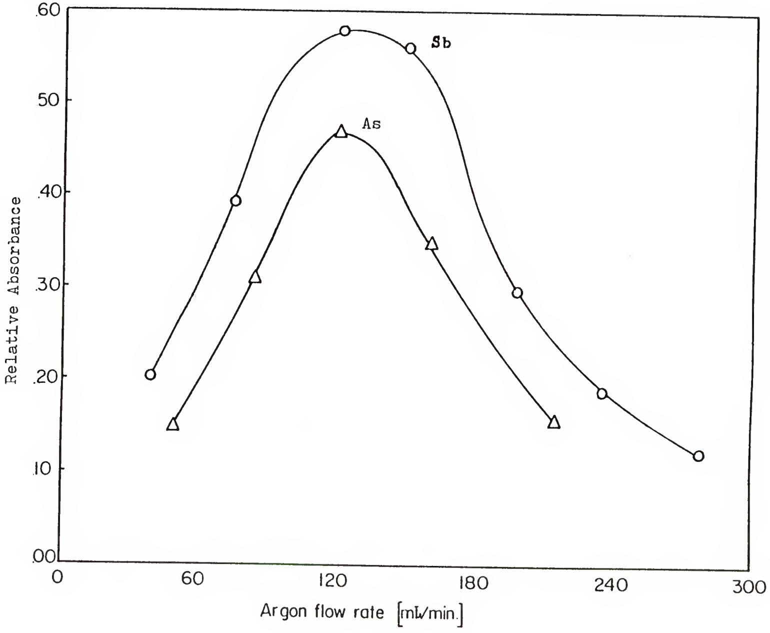
Sb
As
.60
.50
.40
.30
.20
.10
.00
Relative Absorbance
0
60
120
180
240
300
Argon flow rate [mL/min.]

Figure 32. Effect of trapping time on peak height absorption signal for collection mode-hydride generation-long absorption cell atomic absorption spectrometry. Legend: Δ, 10 ng As; o, 10 ng Sb. Experimental condition: absorption wavelengths, As = 197.2 nm and Sb = 217.5 nm.

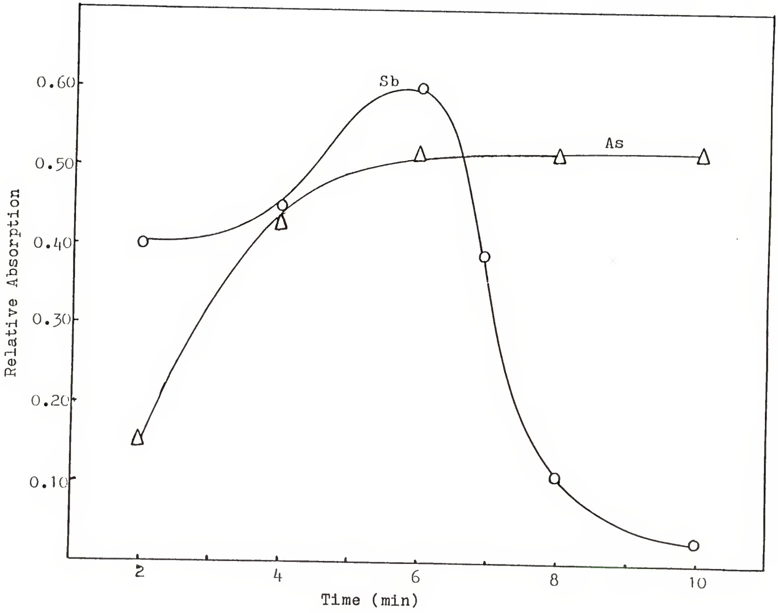
Relative Absorption
0.60
0.50
0.40
0.30
0.20
0.10
Sb
As
2
4
6
8
10
Time (min)

decreases dramatically after 6 min and approaches zero at 10 min. To explain this divergence, two more experiments were conducted. Figure 33 shows the effect of two sequential U-tubes on the relative absorbance for three trapping times. The first U-tube was connected directly to the silica gel drying tube, and the second U-tube connected the sample gas inlet tube to long absorption cell. For a 6-min trapping time, only the first U-tube shows stibine signal; for an 8-min trapping time, only the first U-tube shows stibine signal, but the signal decreases; for a 10-min trapping time, the signal from the first U-tube almost disappears; while the signal from the second U-tube is detectable. Similar experiments were repeated several times, and two liquid N_2 solutions were removed alternately. However, the same results were obtained. If the decreased signal in the first U-tube is totally due to sublimation of SbH_3, the signal in the second U-tube should have been much higher. In fact, the signal in the second U-tube is only detectable, which suggests the effect of sublimation is of no importance.

Figure 34 shows plots of microwave emission signal vs reaction time for hydrogen and stibine. Stibine is a very unstable gas; the m.p. and b.p. of stibine are -88°C and -18.4°C. According to Pfatt (71), the smaller the concentration of free hydrogen is present, the faster the decomposition. In Figure 35, the ratio of the remaining

Figure 33. Effect of trapping time and U-tube traps on 10 ng of Sb (217.5 nm) for collection mode-hydride generation-long absorption cell atomic absorption spectrometry. Legend: a, 6 min trapping time of SbH_3 in coolant; b, 8 min trapping time of SbH_3 in coolant; c, 10 min trapping time of SbH_3 in coolant; 2, second U-tube removed from coolant first; 1, next first U-tube removed from coolant.

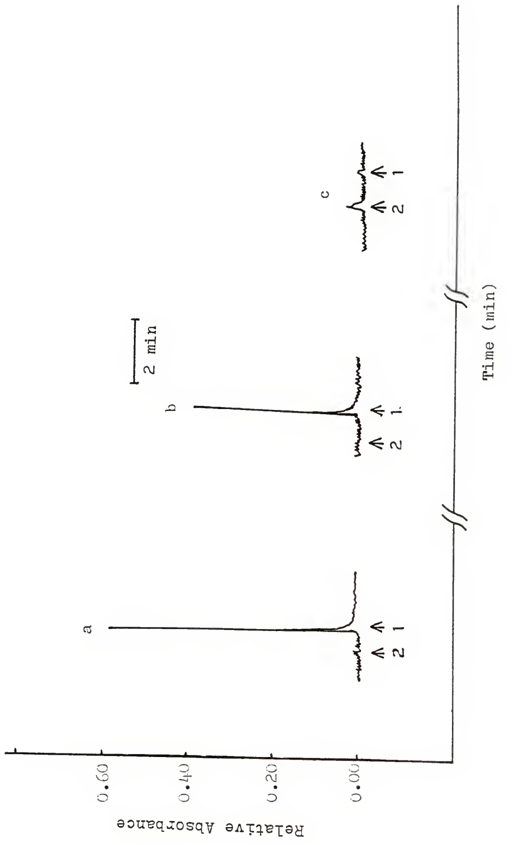
Relative Absorbance
0.60
0.40
0.20
0.00
a
b
c
2 min
2
1
Time (min)

Figure 34. Emission signals of H_2 and SbH_3 as a function of $NaBH_4$/HCl reaction time.

Legend: a, H_2; b, SbH_3 (1 µg); c, SbH_3 (blank). Experimental conditions: emission wavelengths; H = 656.2 nm; Sb = 217.5 nm.

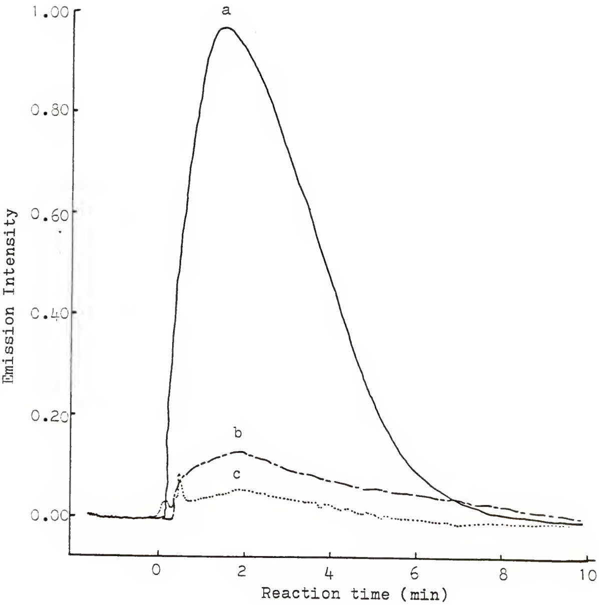
a
b
c
1.00
0.80
0.60
0.40
0.20
0.00
Emission Intensity
0
2
4
6
8
10
Reaction time (min)

hydrogen to total amount of hydrogen is only 2.8% after 6 min. Taylor (72) and Tamaru (73) reported that the deposited stibine film acts catalytically in the decomposition of the stibine. If the signal in the first U-tube decreased due to sublimation of stibine, the signal in the second U-tube should be much higher. The low absorption signal at 10 min thus is possibly explained by major effect of decomposition and minor effect of sublimation of stibine. The trapping time limited the sampling rate of the method. In our case, about six samples per hour were possible because extra time was needed to prepare for the next sample and a helium gas purge time of ~ 2 min was required to remove oxygen in the system before each run.

Interelement Interferences

Interelement (As and Sb) interferences obtained by us and other workers are summarized in Table 18. Figure 35 shows the relationship between relative absorbance and concentration ratio of interferent to analyte in our experiments. The interference effect of As on the determination of Sb is similar to the work of Crock et al. (74). Samples with different matrices may result in variation of permissible concentration ratio. The interference of Sb on the determination of As in our case is opposite to other people's work (74-77). Thiele (78) likewise obtained a similar effect to ours; he concluded

Table 18. Permissible Concentration Ratio of Interferent, I, to analyte, A (I/A).

As/Sb	Sb/As	Sample Source	Ref.
10	6	soil	75
4	2	deionized water	76
100	1000	geological materials	74
200	2000	sea water	77
100	1	deionized water	our work

Figure 35. Effect of interferent on the determination of analyte (10 ng). Legend: Δ, Sb on As; o, As on Sb. Experimental conditions: absorption wavelengths, As = 193.7 nm and Sb = 217.5 nm.

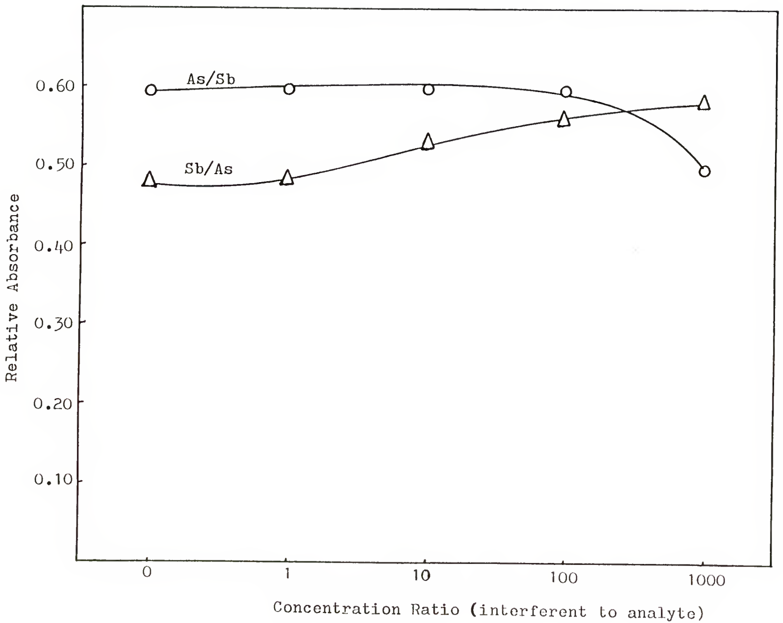
As/Sb
Sb/As
Relative Absorbance
0.60
0.50
0.40
0.30
0.20
0.10
0
1
10
100
1000
Concentration Ratio (interferent to analyte)

that more arsine was formed when a little antimony chloride was present in the solution. Arsine was detected by the well-known Marsh method (79).

Furnace Temperature Effect

Furnace temperature was measured by an optical pyrometer and a W/Re thermocouple; these two methods gave results within ± 50°C of each other. Figure 36 shows the plot of the absorption signal vs furnace temperature for As and Sb. It is obvious that the arsine and stibine dissociate and atomize as the temperature increases above 1100-1200°C. The appearance temperatures for arsine and stibine occur at about 900°C, which are the same as in the paper by Haring, Delft, and Bom (75).

Inner Tube Effect

The effect of an inner tube on the absorption signal is shown in Figures 37 and 38. Signals with alumina and quartz inner tubes are about the same; however, the signal without the inner tube (with graphite tube alone) is greatly suppressed because graphite can form intercalation or lamellar compounds easily. In addition, the inner diameter of the graphite tube is larger than that of the alumina and quartz tubes (6.5 to 4.5 mm), and the signal with graphite tube should decrease 30% according to Equation 20.

Cedergren et al. (80) showed that 45% of ^{74}As was left after pretreatment of the regular graphite tube at

Figure 36. Effect of furnace temperature on the absorption signal for As 10 ng (Δ) and Sb 10 ng (○) with long absorption cell atomic absorption spectrometry. Experimental conditions: absorption wavelengths, As = 193.7 nm and Sb = 217.5 nm.

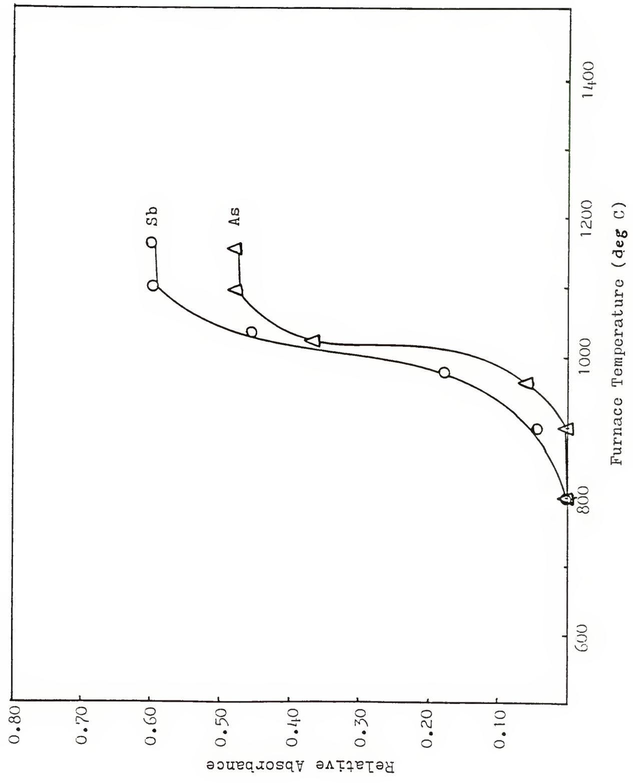
Relative Absorbance
0.80
0.70
0.60
0.50
0.40
0.30
0.20
0.10
600
800
1000
1200
1400
Furnace Temperature (deg C)
Sb
As

Figure 37. Effect of inner tube in long absorption cell on the absorption signal of Sb (10 ng). Legend: a, with alumina inner tube; b, with quartz inner tube; c, graphite tube alone. Experimental conditions: wavelength, Sb = 217.5 nm.

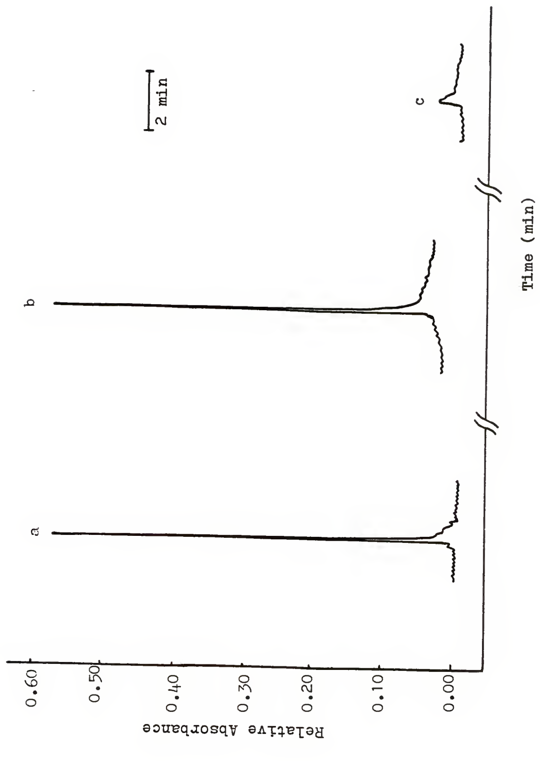
a
b
c
2 min
0.60
0.50
0.40
0.30
0.20
0.10
0.00
Relative Absorbance
Time (min)

Figure 38. Effect of inner tube in long absorption cell on the absorption signal of As (10 ng). Legend: a, with alumina inner tube; b, with quartz inner tube; c, graphite tube alone. Experimental conditions: wavelength, As = 193.7 nm.

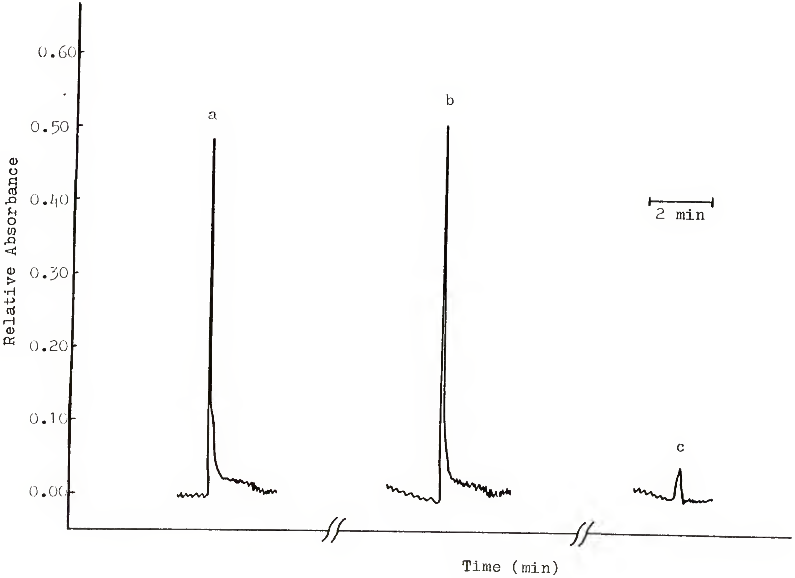
Relative Absorbance
0.60
0.50
0.40
0.30
0.20
0.10
0.00
a
b
c
2 min
Time (min)

1460°C for 90 s. More recently, Sturgeon et al. (81) combined hydride generation system with subsequent trapping in the graphite furnace. The recovery was about 75% at 900°C for 30 s; hydride was further atomized at constant temperature (2600°C). In our laboratory, the atomization temperature for As and Sb is about 1200°C; thus the decreasing absorption signal when only the graphite heater tube was used can now be explained because a certain amount (between 45% and 75%) of analyte was left in the graphite tube. The importance of using an inner tube to avoid reactions between analytes and graphite is obvious.

Welz and Melcher (82) discussed the pronounced influence of the quartz cell surface on the absorption signal. A cleaning procedure with HF was frequently needed because the quartz cell would be contaminated by sample components and would result in low sensitivities. The alumina inner tube worked quite well in our laboratory. The sensitivity did not change much after over 300 heating cycles, and no cleaning step was required.

Zeeman Effect

The long absorption cell was placed inside a modified magnet, and the Zeeman effect was applied to allow background correction. Figures 39 and 40 show absorption signals of 10 ng of As and Sb with and without the Zeeman effect. The smaller signals (with Zeeman correction) are due to absorption line shifts. The Zeeman splitting

Figure 39. Absorption signal for As (10 ng) in long absorption cell without the Zeeman effect (a) and with the Zeeman effect (b). Experimental conditions: wavelength, As = 193.7 nm.

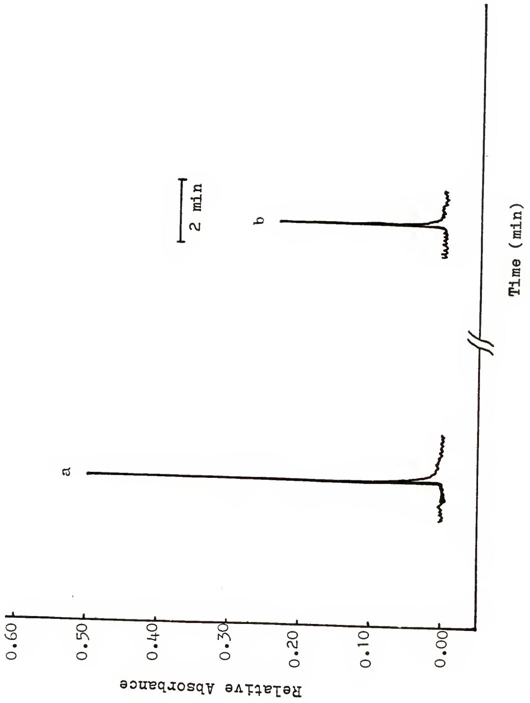
0.60
0.50
0.40
0.30
0.20
0.10
0.00
Relative Absorbance
a
b
2 min
Time (min)

Figure 40. Absorption signal for Sb (10 ng) in long absorption cell without the Zeeman effect (a) and with the Zeeman effect (b). Experimental conditions: wavelength, Sb = 217.5 nm.

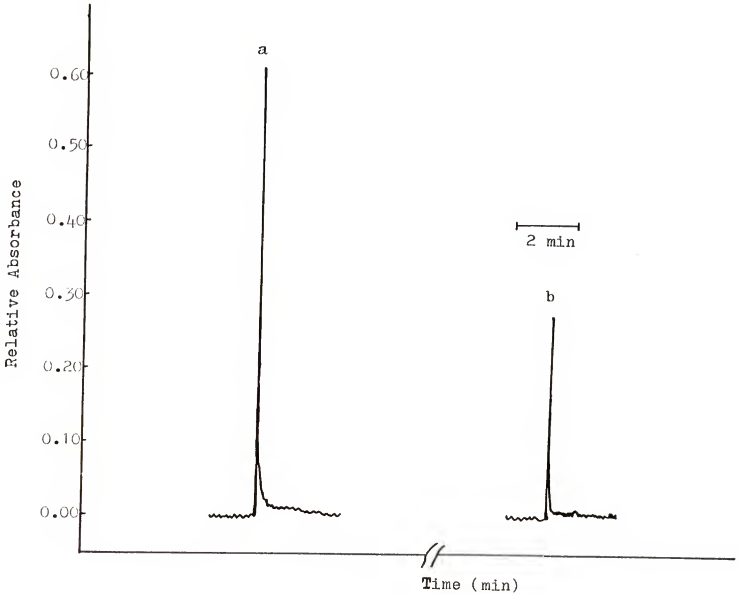
a
b
2 min
0.60
0.50
0.40
0.30
0.20
0.10
0.00
Relative Absorbance
Time (min)

pattern is shown in Figure 41. Both absorption lines (As 193.7 nm and Sb 217.5 nm) are $^4S_{3/2}$ - $^4P_{3/2}$ transition. The Zeeman shift resulted in no central line (see Figure 41, calculation of Zeeman shift is based upon 10 KG magnetic field) in the absorption pattern, and thus the sensitivity decreased when 193.7 nm and 217.5 nm were used as absorption wavelengths for As and Sb, respectively (83); the decrease is due to a poorer overlap of the source line with the absorption profile.

Because the background signal could be attained by running the blank solution with the same procedures as in the hydride generation system, Zeeman correction was not necessary. In future work, however, Zeeman correction will be indispensable to avoid interference of molecular absorption, background, and particulates scattering, when sample is heated and vaporized before being introduced into the atomization region.

Atomization Mechanism

There are two proposed atomization mechanisms for arsine and stibine. In both mechanisms, the appearance temperature occurred at about 900°C. One mechanism involves the collision of MH_3 (M = As or Sb) with free hydrogen radicals by Welz and Melcher (32):

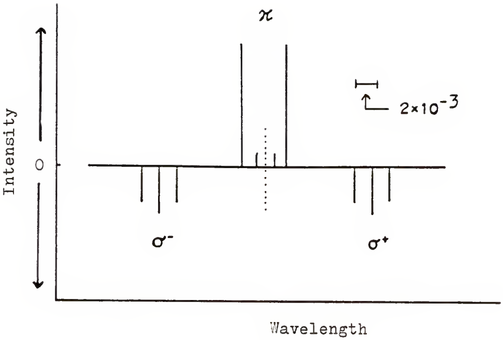

Figure 41. Zeeman splitting pattern for As 193.7 nm and Sb 217.5 nm; broken line, original central line wavelength for As 193.7 nm and Sb 217.5 nm. Adapted from (83).

$$MH_3 + H \rightarrow MH_2 + H_2$$

$$MH_2 + H \rightarrow MH + H_2$$

$$MH + H \rightarrow M + H_2$$

The other mechanism by Akman et al. (84) involves the thermal dissociation of M_4 and M_2 (M = As or Sb):

$$MH_{3(g)} \rightarrow M_{(s)} \rightarrow M_{4(g)} \rightarrow M_{2(g)} \rightarrow M_{(g)}$$

Welz and Melcher (82) suggested the collision mechanism based upon the considerable absorption signal differences (0.7 to 0.0 absorbance unit) when cylinder arsine (3 µL ≈ 50 µg As) was detected with and without the $NaBH_4$/HCl solution in the reaction vessel. In the former case, excess hydrogen was present due to the $NaBH_4$/HCl reaction in blank solution. Their peak height reproducibilities were not good and depended on the speed of arsine injection. Their studies utilized the direct transfer mode, and so excess hydrogen existed during the first few minutes as shown in Figure 34. In our laboratory, signals were measured by the collection mode, so the hydrogen already decreased to 2.8% of total hydrogen after 6 min. Moreover, a similar plot to the one in Figure 36 was obtained when cylinder arsine was directly introduced into the long absorption cell, in which no excess hydrogen was introduced. Therefore, the collision mechanism is not likely to be responsible for atom formation.

Akman (84) proposed that arsine is first decomposed into solid arsenic on the graphite surface. In our experiment, an alumina inner tube was used to avoid the direct reaction of analytes vapor and graphite surface. This is because arsine (or stibine) can easily decompose into metallic arsenic (or antimony) when the temperature reaches above 250°C (79). According to the literature (85-87), two more facts can be found. First, the heat of vaporization of arsenic as As_2 or As_4 is less than that of the monomeric form of As; consequently, vaporization should begin as As_2 or As_4. Second, the decomposition of As_4 to As_2 occurs at 630K (86), which is about the same as the ashing temperature. These facts account for the thermal dissociation mechanism most likely being responsible for atom formation.

Analytical Useful Range (AUR)

Figures 42 and 43 show the analytical useful ranges of As and Sb for three different techniques: namely, the long absorption cell AAS, flame AAS, and conventional GFAAS. The analytical useful range is the range of analyte concentration or amount when the relative random error is 0.05 or less.

Figure 42. Analytical calibration curves for As. FAA, flame AAS; ZFAA, flame AAS with Zeeman effect; LAA, long absorption cell AAS; ZLAA, LAA with Zeeman effect; GFA, conventional graphite furnace AAS; (full line), peak height absorption signal; (dash line), peak area absorption signal.

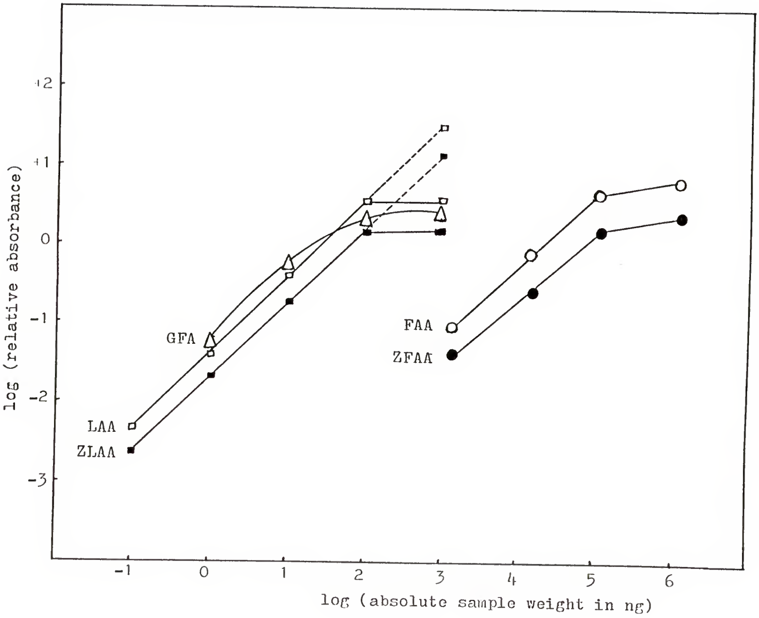
+2
+1
0
-1
-2
-3
log (relative absorbance)
-1
0
1
2
3
4
5
6
log (absolute sample weight in ng)
LAA
ZLAA
GFA
FAA
ZFAA

Figure 43. Analytical calibration curves for Sb. FAA, flame AAS; ZFAA, flame AAS with Zeeman effect; LAA, long absorption cell AAS; ZLAA, LAA with Zeeman effect; GFA, conventional graphite furnace AAS; (full line), peak height absorption signal; (dash line), peak area absorption signal.

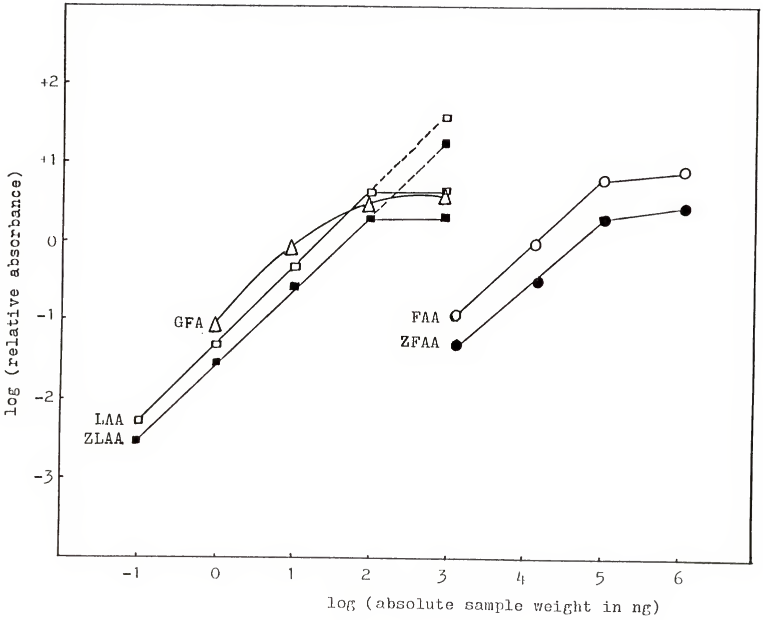
+2
+1
0
-1
-2
-3
log (relative absorbance)
GFA
LAA
ZLAA
FAA
ZFAA
-1
0
1
2
3
4
5
6
log (absolute sample weight in ng)

The flame AAS technique is simple, fast, and more suitable for ppm concentration range measurements. The AUR is about 2 orders of magnitude.

On an absolute mass basis, detection limits of conventional GFAAS are ~ 1000 times more sensitive than the flame technique; however, extensive chemical and physical interferences limit its use. The analytical range is not very large, a little less than 2 orders of magnitude. The atomization mechanism is different from the ones postulated by hydride decomposition; analytes are converted first into their metal oxides (As_2O_3 or Sb_2O_3) during the dry and ash steps. The following mechanism is suggested by Akman (34) for the formation of gaseous As and Sb atoms:

$$As_2O_{3(s,l)} \xrightarrow{\text{vap.}} 2AsO_{(g)} + \frac{1}{2}O_{2(g)}$$

$$AsO_{(g)} \xrightarrow{\text{dissoc.}} As_{(g)} + \frac{1}{2}O_{2(g)}$$

Our long absorption cell AAS, with an independent sample introduction system, avoids interferences of the analyte-graphite tube interactions. The concentration range spans 3 to 4 orders of magnitude depending on whether peak height or peak area absorbance was measured. Figure 44 shows the absorption signals of 100 ng/mL and 1000 ng/mL of Sb. Peak heights are about the same, while peak area

Figure 44. Antimony absorption signal (217.5 nm) for 100 ng Sb (a) and 1000 ng Sb (b) in long absorption cell.

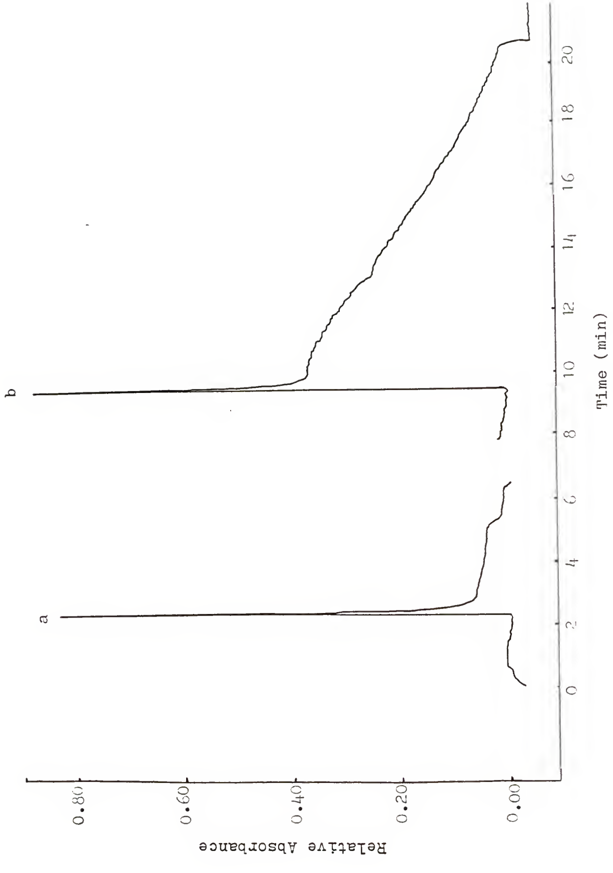
a
b
Relative Absorbance
0.80
0.60
0.40
0.20
0.00
Time (min)
0
2
4
6
8
10
12
14
16
18
20

ratio is 9.4 for 1000 ng/mL Sb to 100 ng/mL Sb. The broad shoulders of the signals may be explained by the specific desorption rate of stibine from the glass bead surfaces in the U-tube.

CHAPTER IV
SUMMARY AND CONCLUSIONS

In the first part of this research, it was shown that the freeze preconcentration process had both advantages and disadvantages regarding various kinds of samples. In the second part of this investigation, the long absorption cell was proven to work well with the hydride generation system.

Freeze Preconcentration Method

For inorganic toxic species, such as As and Pb, the freeze preconcentration technique can be applied with good success to deionized water samples. However, the studies with tap water are poor, and the low recoveries suggest further study.

As for organic species, such as $C_2H_4Br_2$, the freeze concentration process cannot provide reproducible results, because $C_2H_4Br_2$ itself easily escapes from the solution.

Speciation studies of $PbHAsO_4$ and $C_2H_4Br_2$ were carried out. Both studies suggested that the freeze preconcentration technique did not result in a change in the chemical forms of these analytes. However, quantitative determinations of these two species in tap water and other samples were extremely low, and so the freeze preconcentration approach is not recommended for analytical use.

Long Absorption Cell AAS

The long atomic absorption cell which is described and evaluated in this work, is inexpensive and easy to use. In view of the results presented in the above section, this long absorption cell works well with the hydride generation system. More work is needed, however, in order to completely understand the potential of this two-stage furnace concept. For example, research is needed on the vaporization of solid or liquid samples in a quartz cup as shown in Figures 7 and 8 in Chapter II or in a separate electrothermal atomizer, on the transport efficiency, and the capability of speciation. The advantages described for this long absorption cell furnace have to be weighed against the disadvantages of its complexity compared to the Massmann furnace equipped with a L'vov platform.

Optimum hydride reaction, trapping and carrier gas flow rate conditions for arsine and stibine were studied. Interelement interferences, furnace temperature, presence of an inner tube, and Zeeman background correction effects were investigated. Comparisons between conventional flame atomic absorption spectrometry, conventional graphite furnace atomic absorption spectrometry, and long absorption cell atomic absorption spectrometry were given. Detection limits and analytical useful ranges for As and Sb are 0.2 ng/mL and 0.1 ng/mL and 3 to 4 orders of magnitude for both, respectively. Arsenic and antimony were determined in various NBS reference materials and the results agreed well with the NBS values.

REFERENCES

(1) Muller, J.G. Food Technol. 1967, 21, 49-61.

(2) Deshpande, S.S.; Bolin, H.R.; Salunkhe, D.K. Food Technol. 1982, 36, 68-82.

(3) Thijssen, H.A.C. J. Food Technol. 1970, 5, 211.

(4) Almasi, E.; Perjes, P. Bull Inst. Internat'l. Du Froid 46, Annexe 3, 183, 1966.

(5) Bolin, H.R. 1970, Ph.D. Dissertation, Utah State Univ., Logan, Utah.

(6) Thijssen, H.A.C. J. Appl. Chem. Biotechnol. 1971, 21, 372.

(7) Ney, J.J.; Martin, M.G. Water Res. 1985, 19, 905-7.

(8) Maher, W.A. Sci. Total. Environ. 1983, 26, 173.

(9) Powrie, W.D. J. Chem. Educ. 1984, 61, 340-7.

(10) Shapiro, J. Science 1961, 133, 2063-4.

(11) Shapiro, J. Anal. Chem. 1967, 39, 280.

(12) Smith, G.H.; Tasker, M.P. Anal. Chim. Acta 1965, 33, 559-560.

(13) Kobayashi, S.; Lee, G.F. Anal. Chem. 1964, 36, 2197-8.

(14) Mizuike, A.; Kano, S. Japan Analyst 1968, 3, 354-5.

(15) Himes, R.C.; Miller, S.E.; Mink, W.H.; Goering, H.L. Ind. Eng. Chem. 1959, 51, 1345-8.

(16) Yonehara, N.; Kamada, M. Bunseki Kagaku 1981, 30, 620-2.

(17) Ozisik, M.N. "Heat Conduction"; Wiley: New York, 1975; P 397.

(18) London, A.L.; Seban, R.A. Trans. ASME 1943, 65, 771.

(19) Clyne, T.W.; Garcia, A.; Ackermann, P.; Kurze, W. J. Met. 1982, 34, 34.

(20) Brimacombe, J.K. Can. met. Q. 1976, 15,##ol. 1982, 36, 68-82.

(21) Savage, W.F.; Lundin, C.D.; Aronson, A.H. Welding J. (Research Suppl.) 1965, 44, 175-S.

(22) Clyne, T.W.; Garcia, A. J. Mater. Sci. 1981, 16, 1643.

(23) Tao, L.C. A. I. Ch. E. J. 1967, 13, 165-9.

(24) Santos, R.G.; Garcia, A. J. Mater. Sci. 1983, 18, 3578-3590.

(25) Cheng, K.C.; Inaba, H.; Gilpin, R.R. J. Heat Transfer 1981, 103, 733-8.

(26) Hanamura, S. NBS Special Publ. (US)422 1976, NO. 422, 621-4.

(27) Hanamura, S.; Smith, B.W.; Winefordner, J.D. Canad. J. Spectrosc. 1984, 29, 13-8.

(28) Hanamura, S.; Wang, W.; Winefordner, J.D. Canad. J. Spectrosc. 1985, 30, 46-9.

(29) Duval, C. "Inorganic Thermo-Gravimetric Analysis"; Elsevier: London, 1953.

(30) U.S. Environmental Protection Agency, July 1982, Test Method, Purgeables--Method 624: Environment Monitoring and Support Laboratory; Cincinnati, Ohio, P 624-7 - 624-12.

(31) Hanamura, S.; Smith, B.W.; Winefordner, J.D. Anal. Chem. 1983, 55, 2026.

(32) CRC Handbook of Chemistry and Physics, 62nd ed.; CRC Press: Boca Raton, 1981.

(33) Alkemade, C.T.J.; Milatz, J.M.W. J. Opt. Soc. Am. 1955, 45, 583.

(34) Walsh, A. Spectrochim. Acta 1955, 7, 108.

(35) L'vov, B.V. Spectrochim. Acta 1961, 17, 761.

(36) Massmann, H. II Internationals Symposium "Reinststoffe in Wissenschaft and Technik" (Dresden, 1965), S. 297; Akademie-Verlag, Berlin, 1966.

(37) Woodriff, R.; Stone, R. Appl. Optics 1968, 7, 1337.

(38) Matousek, J.P. Prog. Analyt. Atom. Spectrosc. 1981, 4, 247-310.

(39) Woodriff, R. Appl. Spectrosc. 1974, 28, 413-7.

(40) Holcombe, J.A.; Rayson, G.D. Prog. Analyt. Atom. Spectrosc. 1983, 6, 225-251.

(41) Lawson, S.R.; Dewalt, F.G.; Woodriff, R. Prog. Analyt. Atom. Spectrosc. 1983, 6, 1-48.

(42) Vickrey, T.M.; Buren, M.S. Anal. Lett. 1980, 1465-1485.

(43) Sabbatini, L.; Tessari, G. Annali di Chimica 1984, 74, 779-793.

(44) Zhou, N.G.; Frech, W.; de Galan, L. Spectrochim. Acta 1984, 39B, 225-235.

(45) Chang, C.B.; Chakrabarti, C.L. Prog. Analyt. Atom Spectrosc. 1985, 8, 83-191.

(46) Frech, W.; Cedergren, A.; Lundberg, E.; Siemer, D.D. Spectrochim. Acta 1983, 38B, 1435-1446.

(47) Holcombe, J.A.; Rettberg, T.M. Anal. Chem. 1986, 58, 124R-144R.

(48) Long, S.E.; Snook, R.D. Spectrochim. Acta 1985, 40B, 553-568.

(49) Kahn, H.L.; Schallis, J.E. At. Absorpt. Newsl. 1968, 7, 5.

(50) Holak, W. Anal. Chem. 1969, 41, 1712.

(51) Nakahara, T. Prog. Analyt. Atom Spectrosc. 1983, 6, 163-223.

(52) Schmidt, F.J.; Royer, J.L. Anal. Lett. 1973, 6, 17.

(53) Fernandez, F.J. At. Absorpt. Newsl. 1973, 12, 93.

(54) Nakahara, T. Bunseki Kagaku 1982, 31, 534.

(55) Mandel'shtam, S.L. "Introduction to Spectroscopic Analysis"; Gostek-hizdat: Moscow, 1946.

(56) Raikhbaum, Y.D.; Malykh, V.D. Optika i Spektroskopiya 1960, 9, 425.

(57) L'vov, B.V. "Atomic Absorption Spectrochemical Analysis"; Elsevier: New York, 1970.

(58) Sturgeon, R.E.; Chakrabarti, I.S.; Bertels, P.C. Anal. Chem. 1975, 47, 1240-9.

(59) Koirtyohann, S.R.; Kaiser, M.L. Anal. Chem. 1982, 54, 1515A.

(60) Uthus, E.O.; Collings, M.E.; Cornatzer, W.E.; Nielsen, F.H. Anal. Chem. 1981, 53, 2221-4.

(61) POCO Graphite, Inc. Decatur, Texas 76234, catalog.

(62) Aggett, J.; Aspell, A.C. Analyst (London) 1976, 101, 341.

(63) Inui, T.; Terada, S.; Tamura, H. Fresenius Z. Anal. Chem. 1981, 305, 189.

(64) Welz, B.; Schubert-Jacobs, M. J. Anal. At. Spectrom. 1986, 1, 23-7.

(65) Shaikh, A.U.; Tallman, D.E. Anal. Chem. 1977, 49, 1093.

(66) Chapman, J.F.; Dale, L.S. Anal. Chim. Acta 1979, 111, 137.

(67) Thompson, K.C.; Thomerson, D.R. Analyst (London) 1974, 99, 595.

(68) D'Silva, A.P.; Rice, G.W.; Fassel, V.A. Appl. Spectrosc. 1980, 34, 578.

(69) Thompson, K.C. Analyst (London) 1975, 100, 307.

(70) Andreae, M.O.; Asmode, J.; Foster, P.; Van't, L. Anal. Chem. 1981, 53, 1766-1771.

(71) Pfatt, C.H. Pogg. Ann. 1837, 42, 339.

(72) Taylor, H. Canad. J. Chem. 1955, 33, 838-842.

(73) Tamaru, K. J. Phys. Chem. 1955, 59, 1084-8.

(74) Crock, J.G.; Lichte, F.E. Anal. Chim. Acta 1982, 144, 223-233.

(75) Haring, B.J.; Delft, W.; Bom, C.M. Fresenius Z. Anal. Chem. 1982, 310, 217-223.

(76) Lajunen, L.H.; Merkkiniemi, T.; Hayrynen, H. Talanta 1984, 709-713.

(77) Yamamoto, M.; Urata, K.; Murashige, K.; Yamamoto, Y. Spectrochim. Acta 1981, 36B, 671-7.

(78) Thiele, J. Apoth. Ztg. 1890, 5, 86.

(79) Mellor, J.W. "A Comprehensive Treatise on Inorganic and Theoretical Chemistry"; D. Sc.: F.R.S., 1929.

(80) Koreckova, J.; Frech, W.; Lundberg, E.; Persson, J.; Cedergren, A. Anal. Chim. Acta 1981, 130, 267-280.

(81) Willie, S.N.; Sturgeon, R.E.; Berman, E.E. Anal. Chem. 1986, 58, 1140-3.

(82) Welz, B.; Melcher, M. Analyst 1983, 108, 213-224.

(83) de Loos-Vollebregt, M.T.C.; de Galen, L. Prog. Analyt. Atom. Spectrosc. 1985, 8, 47.

(84) Akman, S.; Genc, O.; Balkis, T. Spectrochim. Acta 1982, 37B, 903-912.

(85) Rubeska, I.; Koreckova, J. XX. CSI and 7. ICAS, Symposium III, Prague, 1977.

(86) Weast, R.C. (Editor). "Handbook of Chemistry and Physics," 56th ed.; CRC Press: West Cork, 1976.

(87) Cottrell, T. "The Strengths of Chemical Bonds"; Butterworths: London, 1960.

BIOGRAPHICAL SKETCH

Weng-Jang Chen-Wang was born on February 6, 1954, in Taipei, Taiwan, Republic of China. She received her B.S. degree in chemistry from the National Tsing-Hua University, Hsinchu, Taiwan, in 1976. After graduation, she spent four years at Taiwan Industrial Technology Institute as a research assistant. In 1980, she enrolled in the Graduate School of the University of Florida.

While working toward the degree of Doctor of Philosophy in analytical chemistry, she served as a teaching and research assistant in the Department of Chemistry.

Mrs. Chen was married to Jen-Chi Chen in August, 1979. She is the mother of one lovely girl, Ida. The author is a member of the American Chemistry Society and the Society for Applied Spectroscopy.

I certify that I have read this study and that in my opinion it conforms to acceptable standards of scholarly presentation and is fully adequate, in scope and quality, as a dissertation for the degree of Doctor of Philosophy.

James D. Winefordner

James D. Winefordner, Chairman
Professor of Chemistry

I certify that I have read this study and that in my opinion it conforms to acceptable standards of scholarly presentation and is fully adequate, in scope and quality, as a dissertation for the degree of Doctor of Philosophy.

John G. Dorsey
Associate Professor of Chemistry

I certify that I have read this study and that in my opinion it conforms to acceptable standards of scholarly presentation and is fully adequate, in scope and quality, as a dissertation for the degree of Doctor of Philosophy.

John E. Singley
Professor of Environmental
Engineering

I certify that I have read this study and that in my opinion it conforms to acceptable standards of scholarly presentation and is fully adequate, in scope and quality, as a dissertation for the degree of Doctor of Philosophy.

Richard A. Yost
Associate Professor of Chemistry

I certify that I have read this study and that in my opinion it conforms to acceptable standards of scholarly presentation and is fully adequate, in scope and quality, as a dissertation for the degree of Doctor of Philosophy.

George B. Butler

George B. Butler
Professor of Chemistry

This dissertation was submitted to the Graduate Faculty of the Department of Chemistry in the College of Liberal Arts and Sciences and to the Graduate School and was accepted as partial fulfillment of the requirements for the degree of Doctor of Philosophy.

December, 1986

Dean, Graduate School